MASTERARBEIT | MASTER'S THESIS

Titel | Title

Optimization and Quality Assessment of Silk Fibroin Sponges for Scaffold-based 3D Cell Culture Model

verfasst von | submitted by

Ceren Okuducu

angestrebter akademischer Grad | in partial fulfilment of the requirements for the degree of

Master of Science (MSc)

Wien | Vienna, 2024

Studienkennzahl lt. Studienblatt | Degree programme code as it appears on the student record sheet:	UA 066 606
Studienrichtung lt. Studienblatt | Degree programme as it appears on the student record sheet:	Masterstudium Drug Discovery and Development
Betreut von | Supervisor:	Ass.-Prof. Mag. Dr. Verena Pichler

Table of Contents

Abstract

Silks show notable characteristics like biocompatibility, biodegradability, and non-toxicity, and elicit a minimal immunological reaction. Their exceptional mechanical properties, compatibility with common sterilization techniques, and simple preparation methods make them ideal biopolymers for various uses, including tissue engineering. Silk fibroin can be applied in various morphological configurations. Silk-based formulations can be e.g. tailored to meet individual needs in terms of size, stability, drug capacity, and release kinetics. Given the numerous benefits, research on silk biomaterial has become significant.

Silk sponges have considerable potential in the development of three-dimensional (3D) models for studying cancer. They function as a flexible in vitro medium for administering pharmaceutical compounds and promoting the regrowth of tissues, all while circumventing negative consequences and reducing the necessity for animal testing. Utilizing silk sponges in 3D cancer models provides a more precise representation of the cell microenvironment compared to traditional two-dimensional (2D) cultures. This enhanced realism allows for the simulation of improved in vivo circumstances, resulting in more precise data on tumor behavior and treatment responses. Silk sponges can greatly improve the accuracy of predictions in preclinical trials by replicating the biomimetic environment of living tissues.

The optimization of silk sponges takes the front stage in this master's thesis. The use of the silk sponge modules enables researchers to study several aspects on cancer studies, including testing the effectiveness of drugs and exploring new treatment interventions. This improvement not only simplifies the research procedure but also offers a flexible and dependable instrument for investigating the intricacies of colon cancer in a more regulated and replicable manner.

To optimize the silk sponges, several critical steps must be taken into account during the production process. This master thesis reveals the effect of salt bed height/silk solution ratio, methanol incubation time, and methanol content on the reproducibility of sponge manufacturing. The study employs a range of analytical methods to comprehensively examine and describe silk sponges. These techniques include visual testing, infrared (IR) measurements, scanning electron microscopy (SEM), porosity and density assessments, water retention, swelling ratio, water-uptake capacity, and enzymatic digestion of silk fibroin using α-Chymotrypsin and Protease enzymes. At the same time, enzymatically degraded silk and irradiated silk protein analysis were examined by Sodium dodecyl-sulfate polyacrylamide gel electrophoresis (SDS-PAGE) and Circular Dichroism (CD) spectroscopy. In vitro cytotoxicity assessment with the MTT assay is used in a high-throughput 96-well plate format to simulate prolonged exposure, stress testing, and leaching in organic solvents based on the HT-29 cell line. In line with these evaluations, the optimized sponge was determined as the sponge exposed to 4.5 ml silk solution, 1.2 cm salt bed height, and 3 ml methanol 2 times.

As an outcome of this work, the optimized sponge was selected for a standardized production process for scaffolds. Additionally, this project contributes to reducing the need for animal testing in preclinical studies, improving the accuracy and consistency of cancer research, and compliance with ethical protocols.

Keywords: silk, silk fibroin, silk sponge, 3D scaffold-based method development

Kurzfassung

Seiden weisen bemerkenswerte Eigenschaften wie Biokompatibilität, biologische Abbaubarkeit und Ungiftigkeit auf und lösen nur eine minimale immunologische Reaktion aus. Ihre außergewöhnlichen mechanischen Eigenschaften, ihre Kompatibilität mit gängigen Sterilisationstechniken und ihre einfachen Zubereitungsmethoden machen sie zu idealen Biopolymeren für verschiedene Anwendungen, einschließlich Tissue Engineering. Seidenfibroin kann in verschiedenen morphologischen Konfigurationen verwendet werden. Auf Seide basierende Formulierungen können z. B. in Bezug auf Größe, Stabilität, Wirkstoffkapazität und Freisetzungskinetik auf individuelle Bedürfnisse zugeschnitten werden. In Anbetracht der zahlreichen Vorteile hat die Erforschung von Biomaterialien aus Seide an Bedeutung gewonnen.

Seidenschwämme haben ein erhebliches Potenzial für die Entwicklung dreidimensionaler (3D) Modelle zur Untersuchung von Krebs. Sie fungieren als flexibles In-vitro-Medium für die Verabreichung von Arzneimitteln und die Förderung des Nachwachsens von Geweben, wobei negative Folgen vermieden und die Notwendigkeit von Tierversuchen reduziert werden. Die Verwendung von Seidenschwämmen in 3D-Krebsmodellen ermöglicht eine präzisere Darstellung der Zellmikroumgebung im Vergleich zu herkömmlichen zweidimensionalen (2D) Kulturen. Dieser erhöhte Realismus ermöglicht die Simulation verbesserter In-vivo-Bedingungen, was zu präziseren Daten über das Tumorverhalten und das Ansprechen auf die Behandlung führt. Seidenschwämme können die Genauigkeit der Vorhersagen in präklinischen Studien erheblich verbessern, indem sie die biomimetische Umgebung von lebendem Gewebe nachbilden.

Die Optimierung von Seidenschwämmen steht in dieser Masterarbeit im Vordergrund. Die Verwendung der Seidenschwamm-Module ermöglicht es den Forschern, verschiedene Aspekte von Krebsstudien zu untersuchen, einschließlich der Prüfung der Wirksamkeit von Medikamenten und der Erforschung neuer Behandlungsmethoden. Diese Verbesserung vereinfacht nicht nur das Forschungsverfahren, sondern bietet auch ein flexibles und verlässliches Instrument, um die Feinheiten des Dickdarmkrebses regulierter und reproduzierbarer zu erforschen.

Um die Seidenschwämme zu optimieren, müssen mehrere kritische Schritte während des Produktionsprozesses berücksichtigt werden. In dieser Masterarbeit wird die Auswirkung des Verhältnisses zwischen Salzbetthöhe und Seidenlösung, der Methanol-Inkubationszeit und des Methanolgehalts auf die Reproduzierbarkeit der Schwammherstellung untersucht. In der Studie wird eine Reihe von Analysemethoden eingesetzt, um Seidenschwämme umfassend zu untersuchen und zu beschreiben. Dazu gehören visuelle Prüfungen, Infrarotmessungen, Rasterelektronenmikroskopie (REM), Bewertung von Porosität und Dichte, Wasserrückhaltevermögen, Quellungsgrad, Wasseraufnahmekapazität und enzymatischer Verdau von Seidenfibroin mit den Enzymen α-Chymotrypsin und Protease. Gleichzeitig wurden enzymatisch abgebaute Seide und bestrahlte Seidenproteine durch Natriumdodecylsulfat-Polyacrylamid-Gelelektrophorese (SDS-PAGE) und Circulardichroismus (CD)-Spektroskopie untersucht. Die In-vitro-Zytotoxizitätsbewertung mit dem MTT-Assay wurde in einem 96-Well-Plattenformat mit hohem Durchsatz durchgeführt, um eine verlängerte Exposition, Stresstests und das Auslaugen in organischen Lösungsmitteln auf der Grundlage der HT-29-Zelllinie zu simulieren. In Übereinstimmung mit diesen Bewertungen wurde der optimierte Schwamm als der Schwamm bestimmt, der 2 Mal 4,5 ml Seidenlösung, 1,2 cm Salzschichthöhe und 3 ml Methanol ausgesetzt wurde.

Als Ergebnis dieser Arbeit wurde der optimierte Schwamm für ein standardisiertes Produktionsverfahren für Scaffolds ausgewählt. Darüber hinaus trägt dieses Projekt dazu bei, die

Notwendigkeit von Tierversuchen in präklinischen Studien zu verringern, die Genauigkeit und Konsistenz der Krebsforschung zu verbessern und die Einhaltung ethischer Protokolle zu gewährleisten.

Stichworte: Seide, Seidenfibroin, Seidenschwamm, 3D-Gerüst-basierte Methodenentwicklung

Acknowledgement

First and foremost, I'd like to thank my supervisor, Ass. -Prof. Mag. Dr. Verena Pichler, for all of her help and advice throughout the internship and thesis process. Her mentorship and counsel supported me during every phase of composing my thesis.

I would also like to express my special thanks to Verena Schwingenschlögl-Maisetschläger for her teachings and support throughout this whole process. I am very happy to have been involved in this project with her, and I am grateful for everything she taught me.

Another thank you goes to Irem Duman and Xavier Monforte Vila, who never withheld their help and answered my questions throughout this process.

I must also express my gratitude to my family and friends for their unwavering support throughout this arduous school year.

1. Introduction

Silk is a protein fiber that is naturally produced by different insects and arachnids. The creation of this structure has two distinct goals in various species: firstly, it acts as a protective outer covering during the transition from larval to adult stages, and secondly, it functions as a method for trapping prey. (1) Spider silk, mulberry silk, eri silk, muga silk, and tussar silk are among the most known varieties of silk. (2)

The principal source of commercial silk is the domesticated mulberry silk moth, *Bombyx mori*, which has been tamed from its wild relative, *Bombyx mandarina*, for thousands of years. (3) Since the insect cannot survive in its natural environment, sericulture and the production of raw silk cocoons have become quite popular as a result of forced evolution. (3)

It was the Yangshao culture of Neolithic China that first began making silk. Silk was originally only worn by the Chinese emperor and other high-ranking officials, but as time went on, wealthier people began to have access to it, and as a result, the business grew significantly. Silk was utilized for musical instruments, fishing lines, bowstrings, and opulent textiles. Over time, it became a currency in the Han dynasty and was even used in trade.

The use of silk, which has grown in significance throughout time, has transcended conventional uses and is currently highly valued within the scientific community. Its potential in these cutting-edge domains has been shown by the acceleration of research on its applications in tissue engineering (TE) and biomedicine in recent years. In this master's thesis, silk structure and its properties and usage areas are explained in detail. In addition to this, optimization and characterization studies were carried out on silk fibroin scaffold-based sponges and the results were included.

1.1. Structural Features of *Bombyx Mori*

Silk is a biopolymer material with a semicrystalline structure. The cocoon of *B. mori* is composed of a singular continuous fiber including two primary proteins: sericin and silk fibroin (SF). (5,6)

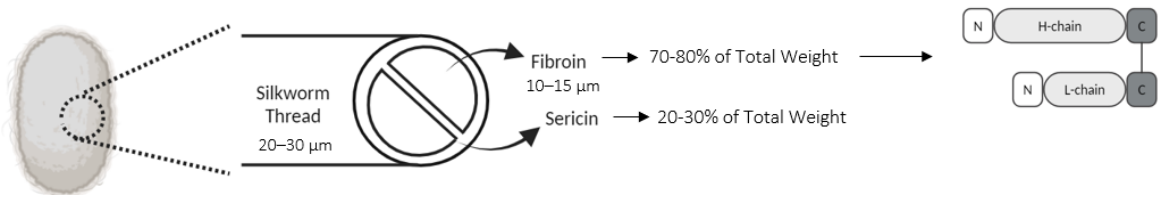

Figure 1: Representative illustration of the silk protein of Bombyx mori, which consists of two main proteins: sericin and fibroin. Silk fibroin is the main component of the silk cocoon structure. It comprises from heavy (H) and light (L) chains.

Silk exhibits an intricate and well-structured composition, consisting of numerous layers and organized in a structured way. Within the spun fiber, there exists a layer of sericin that encompasses two fibroin strands. Each strand has a diameter of 10–15 µm; the spun fiber itself has a diameter of approximately 20–30 µm. The brins comprise fibrils with diameters between 200 and 400 nm. These fibrils then consist of nanofibrils with a 3 to 5 nm diameter. (7) The amorphous and crystalline phases proceed to build up the series of nanofibers. Molecular folding in three dimensions is driven by the fundamental structure of a protein. Proteins undergo a process known as folding, where they adopt specific shapes termed secondary structures. These secondary structures include β-sheets and α-helices. The folding occurs due to the formation of hydrogen bonds between carboxyl groups and amino groups in surrounding regions. The tertiary structure of a protein is its three-dimensional conformation, which is ascertained from the general aggregation and folding of the protein including its secondary structures. The arrangement of several folded protein subunits to create a complex macromolecule is known as a quaternary structure. (1)

Comprising 70–80% of their entire weight, SF is an essential component of *B. mori* cocoons. Maintaining silk's structural integrity depends critically on SF. (8) Two chains make up the structure: the repetitive, heavy (H) chain and the non-repetitive, light (L) chain. Both chains have respective molecular weights of 26 kDa and over 370 kDa. (9) A complex called H-L, consisting of interconnected chains linked by a disulfide bond, can bind P25, a glycoprotein, at a ratio of 6:1 through hydrophobic interactions. (10) Prior to the spinning of the fiber, the native silk solution in the insect gland forms a single micellar unit through the combination of the 6H-L complexes with the glycoprotein P25. (11)

The heavy chain consists of a series of mostly hydrophobic amino acids. This series is repeated several times with variants including $(Gly\text{-}Ala\text{-}Gly\text{-}Ala\text{-}Gly\text{-}Ser)_n$, $(Gly\text{-}Ala\text{-}Gly\text{-}Ala\text{-}Gly\text{-}Tyr\text{-}Gly\text{-}Ala\text{-}Gly)_n$ and $(Ala\text{-}Gly\text{-}Val\text{-}Gly\text{-}Tyr\text{-}Gly\text{-}Ala\text{-}Gly)_n$. These repeated sequences can arrange themselves into β-sheet crystallites because to the strong hydrogen bonding between the amines and carboxyl groups on nearby chains, hence producing spun fiber with remarkable mechanical stability. (12) Three separate β-sheet configurations define the protein SF: parallel β-sheet, antiparallel β-sheet, and native β-sheet. Whereas the antiparallel β-sheet exhibits linear and shorter hydrogen bonding, the parallel β sheet displays non-linear and longer hydrogen bonding. (10) Non-repeating amino acid composition of the light chain produces a random-coil arrangement with either minimal or no crystallinity. Two chains have different physical qualities: the heavy chain is stiff and hydrophobic; the light chain is flexible and hydrophilic. The existence of the light chain component clearly influences SF's general behavior. The mechanical properties of silk are attributed to the mixture of rigidity and mechanical stability of crystalline regions and the flexibility of random coil regions. (1)

There are three crystalline polymorphs observed for bulk SF (13): Silk I, belonging to the orthorhombic system, which is still a matter of debate and water-soluble state, and silk II, with a monocline structure mainly composed of antiparallel β-sheets (14,15) which is crystalline silk. Comprising elongated helices, silk III is visible in the air/liquid interface of the fibroin solution. (14,15)

With 20–30% of the total weight, silk sericin makes up the secondary component. (16) To maintain structural integrity, silk sericin envelops the SF fibers in a continuous form. (8) It is composed of a larger amount of polar amino acids, allowing it to have large reactivity and water solubility. (17)

The removal of sericin from silkworm silk is necessary for biocompatibility since it can cause unfavorable immunological reactions in humans. (18) In vitro and in vivo studies indicate that sericin-free fibroin fibers show enhanced mechanical properties than sericin-encased fibroin (19), including a 50% increase in tensile strength, a modulus of up to 15–17 GPa, and a strain at breakage of up to 19%. (2) It is easy to remove sericin explicitly. These two proteins can be distinguished from one another by employing a well-known procedure called degumming, which entails solubilizing sericin in a heated sodium carbonate (Na_2CO_3) bath. This bath cannot solubilize the fibroin, which is therefore recovered as a solid fibrous product.

1.2. Properties of Silk

Among other natural biopolymers, silk stands out for its remarkable mechanical characteristics. The availability of easily accessible functional groups for chemical manipulation enhances its distinct edge even more. Silk also exhibits exceptional biodegradability, biocompatibility, and bioresorbability, which makes it an excellent choice for a variety of biomedical applications.

1.2.1. Mechanical Properties

Among SF fibers remarkable mechanical characteristics are a considerable break strain (4–26%), ultimate strength (300–740 MPa), and toughness (70–78 MJ m^{1}). (10) These qualities exceed synthetic materials including certain collagens, carbon fiber, and Kevlar. Among natural materials including wool,

resilience, elastin, byssus, cotton, synthetic fibers such synthetic rubber and viscose rayon (20,21), SF fibers also show the best strength. In biomaterial engineering, SF scaffolds—despite their great mechanical qualities—usually consist of regenerated silk fibroin (RSF) solutions, which can be brittle and weak without hierarchical and secondary structures. (22) Methods to improve the mechanical qualities of RSF-generated silk scaffolds have been investigated. Comparatively to raw SF fibers, dry-spinning methods produced a 28.6% reduced breaking stress. (23) Further improving the qualities include crosslinks, porogens, 3D bioprinting technologies. Strong enough for surgical operations, the generated scaffolds closely reflect the natural tissue being rebuilt, therefore guaranteeing ideal repair conditions. (22)

1.2.2. Biocompatibility

Biocompatibility is crucial for a scaffold to work properly because it allows cells to attach to the scaffold, move inside of it, multiply, and differentiate. (22) After implantation, the scaffold must not cause a major immune response; this is of the utmost importance. (24) Since SF is a naturally occurring polymer, it is known to be biocompatible and biologically inert. (25) In vivo studies using SF have shown blood compatibility since 1989. (26) In 1993, the Food and Drug Administration approved SF for utilization as a biomaterial in sutures. (25) In vitro experiments do not show any appreciable macrophage response to SF films or fibers. (27,28) However, in vivo studies show an inflammatory response to SF films that is similar to collagen. (29)

1.2.3. Biodegradability and Bioresorbability

Biodegradability and bioresorbability are crucial characteristics for effective scaffold materials, as the scaffolds need to be gradually replaced by the patients' own cells and extracellular matrix (ECM) during the recovery process. (30) SF and other enzymatically degradable polymers are non-toxic and do not cause harm to various tissues, organs, or systems. (10) Enzymes bind to the SF scaffolds and initiate their degradation by ester bond hydrolysis. (10,30,31) Enzyme solutions precipitate the breakdown of non-crystalline SF structures, which then crystallize into hydrophobic shapes and disintegrate even more in the presence of enzymes. (10)

Among the proteolytic enzymes that potentially break down SF are protease XIV, collagenase IA, and chymotrypsin. (30, 32,33) Protease XIV derived from *Streptomyces griseus*, is the most common employed enzyme for degrading silk due to its higher SF destruction activity compared to both collagenase IA and chymotrypsin. (10) The methods used in preparation also affect the degradation of SF, thereby resulting in different morphologies of SF particles. (34) Research conducted in vivo on SF porous scaffolds implanted in Lewis rats revealed that the scaffolds broke down in eight weeks and that macrophage degradation completely destroyed the scaffolds after a year. This data illustrates that SF scaffolds possess the characteristics of being both biodegradable and bioresorbable.

Native silk fibers degrade at a slower rate than RSF silk scaffolds due to their higher concentration of ß-sheet secondary structure. (35) The rate of SF degradation and the number of ß-sheet secondary structures show a clear link. (10) Methanol treatment produced RSF films with a greater number of ß-sheet structures (36), whereas slow air-drying produced RSF films with a lower content and faster rates of degradation. (37) It has also been shown that ɣ--radiation hastens the degradation of SF fibers since it induces silk II to become silk I. (38)

1.3. Application of Silk Fibroin

From ancient times, silk has been extensively used to produce a variety of textiles including household furniture, bedding, and clothing. The unique features of silk and extraordinary self-assembly capabilities allow novel uses for silk, including biosensors, bioprinting, regenerative medicine, drug delivery, TE, and medical devices. In following, the application areas of silk fibroin are briefly explained.

1.3.1. Textile

Textile materials are affected by both their visual attractiveness and their practical effectiveness. (39) Silk fibroin fibers are commonly selected for their glossy look, smooth texture, convenient dyeing qualities, exceptional mechanical characteristics, compatibility with living organisms, and capacity to absorb moisture. Conventional dyeing techniques necessitate severe conditions, which lead to the degradation of the characteristics of silk fibers. A recent study indicates that intrinsic functionalization methods can be used to provide widespread colors while maintaining the mechanical qualities of the material Antibacterial chemicals can treat silk to provide it with antibacterial qualities, guard against UV radiation, and enable self-cleaning. Antibacterial clothing, sportswear, military uniforms, filtration fabrics, cosmetic textiles, and therapeutic textiles all have silk in great use in their manufacturing. (10)

1.3.2. Surgical Suture

Because of its excellent handling qualities, low bacterial adhesion, and great strength, SF is a commonly used suture material. (40-42) In vivo, SF becomes soluble after 60 days. (43) But because silk is usually braided, it might cause allergic reactions. These reactions are lessened by non-braided sutures because of their smoother surface and lack of crevices for chemicals that cause inflammation. (44) Consequently, it is preferable to employ non-braided silk sutures, which call for stronger and more resilient silk. (45) This is one goal in improving the mechanical qualities of silk. (10)

1.3.3. Therapeutic Agent Delivery

Silk fibroin material is advantageous for carrying therapeutic agents due to its mild processing options, superior mechanical properties, and excellent stabilizing effect. (46,47,48) Therapeutic agents can be surface loaded or bulk loaded in fibroin carriers, depending on the amount of drug and release kinetics in vitro/in vivo. Surface loading refers to the process of applying the agents directly onto native or regenerated fibroin carriers, while bulk loading entails trapping the agents within regenerated fibroin carriers. Opting for bulk loading is advantageous since it permits larger quantities of agents. Therapeutic chemicals are combined with regenerated silk solution and formed into carriers that are mechanically stable. Enzymes that are trapped, such as glucose oxidase, lipase, and horseradish peroxidase, retain significant biological activities even after being stored for 10 months. The release of trapped agents can be regulated by altering the ß-sheet composition and crystallinity of the fibroin, which in turn influences the release profile. Therapeutic drugs are delivered locally, systemically, and cell-wise using fibroin carriers; their mechanical characteristics are therefore quite important in these kinds of delivery. (10)

1.3.4. Optics and Sensing

The greater refractive index and biocompatibility of fibroin make it a promising substrate for optics and sensors, which is now being investigated. (10) Its mechanical and lightweight characteristics render it well-suited for the purpose of directing the propagation of light waves. (49) Fibroin has been employed in a diverse range of optical and sensing components, such as waveguides, diffraction gratings, lens arrays, electrical sensors, oxygen sensors, pH sensors, glucose sensors, and food sensors. (48,50-53)

1.3.5. Tissue Engineering

Since the FDA recognized silk as a biomaterial in 1993, numerous devices produced from silk have been approved by the agency for use as tissue augmentation injectables, ligament grafts, and bioresorbable surgical meshes, among other applications. (54, 55) Silk fibroin has a wide range of uses in tissue engineering that fall into several categories (see *Figure 2*). These categories cover a range of particular applications, highlighting the SF's adaptability in this area which is mentioned in the following sections.

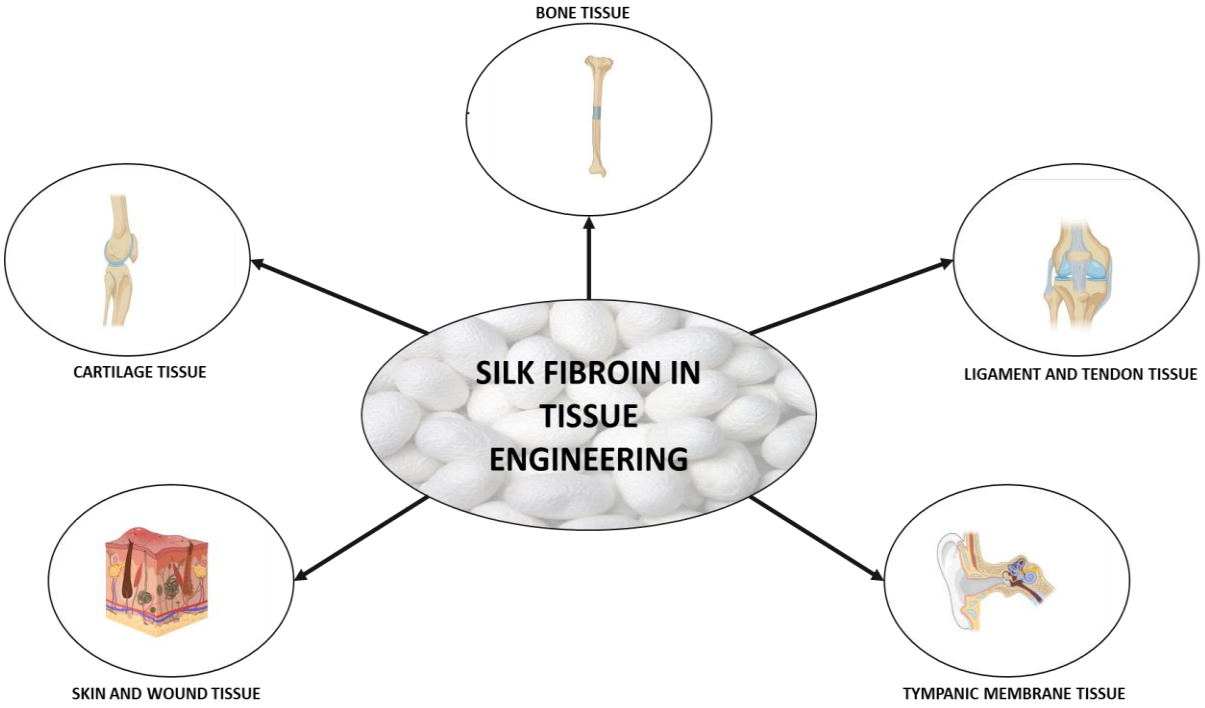

Figure 2: Silk fibroin application areas in tissue engineering generally investigated under several tissues. These tissues consist of: bone, cartilage, ligament and tendon, tympanic membrane, and skin and wound tissue.

1.3.5.1. Bone Tissue Regeneration

Bone is a specialized connective tissue combining 60% inorganic matrix with 35% organic components. Its main elements are hydroxyapatite (56,57) and collagen, which improves the hierarchical architecture and strength of bone. (58) Designed scaffold materials for bone TE should guarantee matrix toughness and allow for the ECM deposition. RSF have been widely studied for their high toughness, mechanical strength, and biocompatibility. In vitro and in vivo RSF scaffolds have been demonstrated to induce osteogenic differentiation of Human mesenchymal stem cells (HMSCs). (60)

Demineralized bone matrix (DBM) powder or particles mostly consist of collagen and Bone morphogenetic protein, which have osteoinductive and osteoconductive characteristics. RSF as a carrier for loading DBM has been shown to promote osteogenesis in mice together with bone marrow stem cells. (61) Rapid and thorough vascularization is required for successful bone regeneration. (10)

1.3.5.2. Cartilage Tissue Regeneration

Among connective tissues, cartilage is one without blood vessels or nerves. Rich ECM surrounds it and lacks the natural ability for self-healing following damage or degeneration. (10) Mostly consisting of collagen and proteoglycans, the ECM of cartilage helps to provide mechanical characteristics of tissues in vivo. (63,62) Maintaining and sustaining this tissue is a crucial component of TE. (10) SF scaffolds can be used to enhance the production of cartilaginous ECM (38), and can be fabricated into different morphologies due to their tuneable properties. (64) Combining porous RSF scaffolds with HMSCs can create zonal structures akin to native cartilage tissue; Insulin-like Growth Factor I can stimulate many progenitor cell growths. (65) Other natural biopolymers, such as chitosan, which can give sufficient support to chondrocytes due to existing glycosaminoglycan residues (66), can be mixed with RSF to form biocompatible cartilage constructions. RSF-Gelatin, a partial derivative of collagen, can also promote chondrogenic differentiation. (67) Thus, it has been demonstrated in numerous studies that combining RSF with synthetic, natural, and biomaterials can improve scaffolds used in the regeneration of ligament and tendon connective tissues.

1.3.5.3. Skin and Wound Tissue Regeneration

The skin serves as a crucial barrier against pathogenic pathogens, comprising mostly of the epidermis and dermis layers. (10) Research has demonstrated that RSF biomaterials have an impact on the adherence of keratinocytes and fibroblasts. These biomaterials are commonly used in tissue engineering for skin regeneration. (68) RSF films were inserted into complete skin defects in rabbit and porcine models, resulting in decreased healing time and superior skin regeneration when compared to commercially available wound dressings. RSF mats, which have been coated with antibacterial silver nanoparticles, can serve as antimicrobial wound dressings to effectively hinder the growth of *Staphylococcus aureus* and *Pseudomonas aeruginosa.* (69)

Chitosan is widely used in skin TE due to its biocompatibility, biodegradability, and antimicrobial ability. (70) It promotes collagen formation from fibroblast cells, increasing the tensile strength of regenerated tissue in the defected area. (71,72) Alginate dialdehyde improves cell proliferation and attachment and exhibits reduced toxicity when employed as a crosslinking agent. (73) Therefore, it has been proven that composite RSF scaffolds can be integrated with both natural and synthetic materials to enhance mechanical properties, minimize the likelihood of infection, and facilitate ideal wound healing.

1.3.5.4. Tympanic Membrane Tissue Regeneration

Between the middle ear and the outer ear lies a structure known as the tympanic membrane (TM), which is a transparent structure that is responsible for receiving sound vibrations and protecting the middle ear. The epidermal outer layer, the fibrous middle layer, and the mucosal inner layer are constituents of this structure. These layers are mostly made up of keratinocytes, fibroblasts, and collagen. TM perforations commonly result from otitis media or traumatic ruptures (10). Failure to restore them within a three-month timeframe can result in auditory impairment and recurring infections. RSF is a suitable material for TM tissue engineering because it facilitates the proliferation and migration of keratinocytes produced from human TM cells (10). Research has demonstrated that RSF films can effectively mend tympanic membrane perforations and expedite the process of regeneration, resulting in quicker restoration of hearing. Additionally, they have a strong ability to transfer acoustic energy and offer impressive tensile strengths when it comes to cartilage. This suggests that they have the potential to be used for regenerating TM perforations in vivo. (74)

1.3.5.5. Ligament and Tendon Tissue Regeneration

Ligament and tendon tissues are composed of collagen and fibrocytes, which are dense fibrous connective tissue that can be easily impaired and lack natural regeneration. (75,76) Due to their unique mechanical properties and structural integrity, RSF scaffolds have become a preferred biopolymer for the regeneration of ligaments and tendons. (77) The first RSF matrix was created as an anterior cruciate ligament in 2002. (78) Since then, scientists have developed knitted scaffolds based on SF for regeneration, which encourage the healing of the scaffold-ligament interface in the medial collateral ligament of rabbits. (79) Ligament and tendon connective tissue restoration can be improved by combining RSF with synthetic and natural biomaterials.

1.4. Morphologies of Silk Biomaterials for Tissue Regeneration

Silk proteins can be processed into a wide range of morphologies, such as hydrogels, films, mats, synthetic fibers, sponges, and even 3D bioprinting. (80) Application areas vary considerably on tissues and cells based on the regenerated morphologies' nature. The subject of this study is silk sponges, which are networked porous structures that in vitro and in vivo resemble physiological environments. Due to their 3D structure, they promote waste and nutrition movement by perfusion or diffusion in bioreactor setups, as well as cell adhesion, proliferation, and migration. (81) In addition, all silk fibroin morphologies are described in this section.

1.4.1. Native Silk Structures

Silk fibers can be utilized in tissue regeneration by creating twisted structures like rope, cable, braided, and textured yarns. (82) Cocoons can serve as cell supporting templates, maintaining the porous mat's structure. Knitted silk structures can reinforce 3-D porous scaffolds, improving their mechanical properties for load-bearing applications like ligaments.

1.4.2. Regenerated Silk Fibroin Morphologies

Concentrated solutions of chaotropic salts, such as LiBr, $CaCl_2$/ethanol/water, LiSCN, or ionic liquids, are used in the manufacture of silk solutions in order to regenerate various silk formats. (83-85) Silk fibers that are not mulberry-based are frequently insoluble in these solutions. (86,87) For this reason, they are not widely used in TE applications. Regenerated silk fibers are quite diverse which can be summarized as *Figure 3*.

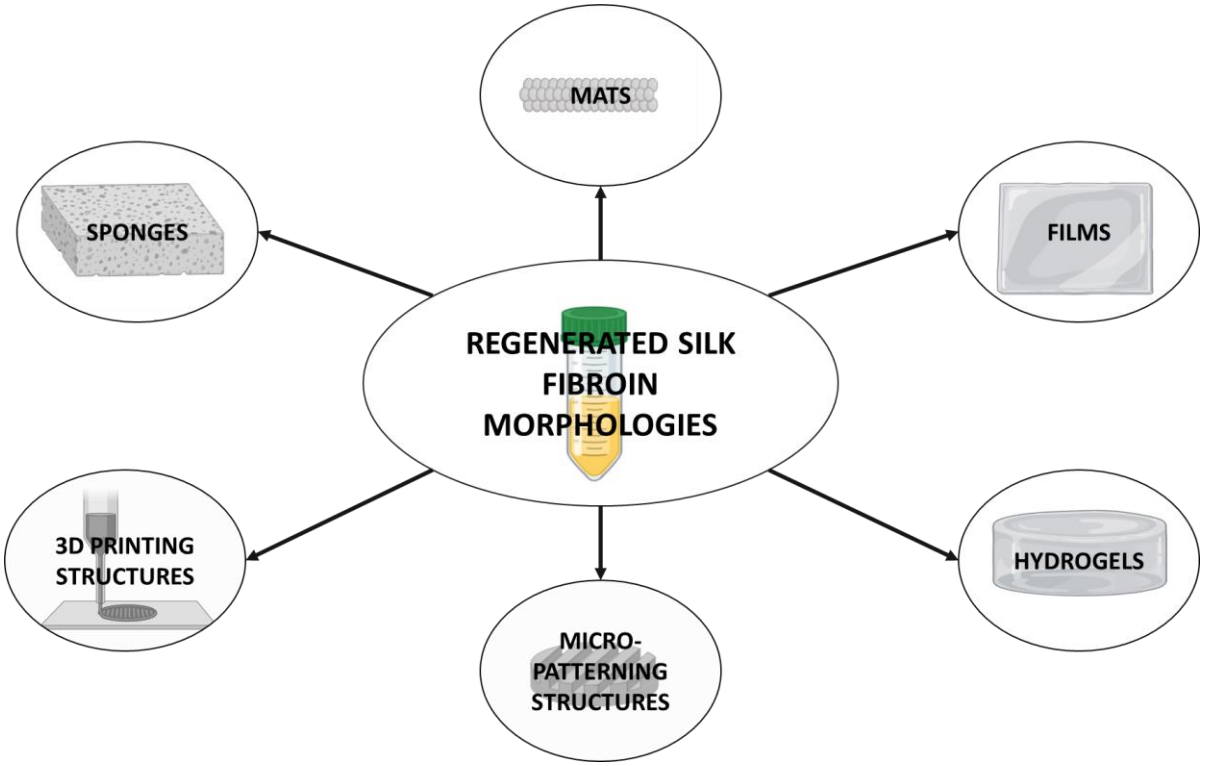

Figure 3: Regenerated SF morphology types include: sponges, mats, films, hydrogels, micro-patterning, and 3D printing structures.

1.4.2.1. Films

SF films can be produced by casting aqueous, acidic, and ionic silk solutions. (88,89) For the purpose of obtaining films, procedures such as spin coating, Langmuir-Blodgett processes, and manual or spin-assisted layer-by-layer deposition are utilized. (88,89,90) The improvement of β-sheet crystallinity is achieved through the utilization of several techniques such as controlled drying, water annealing, stretching, and alcohol immersion. (10,91-93) In order to achieve directed cell growth or optical features, it is vital to successfully control surface characteristics. Cast films are guaranteed to be stable thanks to the utilization of lithography and other advanced printing techniques. (10,94) These properties are achieved through applying these techniques.

1.4.2.2. Mats

Electrospinning, wet spinning, and dry spinning are the three most common processing techniques that are utilized in the production of RSF mats, also known as artificial silk fibers. Using the electro spinning method, it is possible to manufacture polymeric nanofibrous scaffolds. When applied in TE applications,

these scaffolds can more closely match the natural fibers that are found in the extracellular matrix. (80) Due to their wide surface area and porous structure, electro-spun silk nano-fiber mats are advantageous for a variety of applications, including nerve guides, blood vessel grafts, and cell seeding procedures. (93) Wet spinning or micro-fluidic solution spinning can be used to create regenerated silk fibers, which can be produced on a larger scale than nano-fibers. (10) Dry-spinning is more environmentally friendly than the previous techniques because it does not involve the use of coagulation baths or organic solvents. (80) Advantages of regenerated silk fibers include the ability to adjust morphology and properties based on application and the incorporation of bio-molecules during regeneration from silk solution. (10)

1.4.2.3. Hydrogels

Hydrogels are 3D polymer networks that expand when exposed to water. They are capable of being cross-linked either chemically or physically, and they are effective in encapsulating and seeding cells in the process of developing applications for TE. (95) As seen by the increasing number of silk-based publishing records, RSF hydrogels have been utilized in connection with a variety of RSF morphologies, which have been gaining popularity up to this moment.

They are induced both physically and chemically. By varying the pH, temperature, protein concentration, and the addition of precipitating agents, RSF hydrogel gelation kinetics can be changed from minutes to hours. (22) Silk hydrogels are formed through a sol-gel transition of aqueous silk fibroin solution, accelerated by protein concentration, temperature, and Ca^{+2} addition. (96-99) They are useful for injectable or non-injectable delivery systems and have mechanical properties suitable for load-bearing TE, such as cartilage regeneration, and can be used for scaffolds. (10,100) Also, it provides multiple options for the delivery of cells and cytokines in TE. (80)

1.4.2.4. Micro-Patterning Structures

Cellular behavior is greatly influenced by the many micro- and nano-scale topologies that make up the ECM. It is essential to model these topologies in order to guarantee appropriate cell behavior both in vitro and in vivo (80). It has been demonstrated that RSF's micro-patterning structure influences adhesion, proliferation, and migration of cells. In recent years, there has been a significant rise in interest in the technology of micro-patterning, which enables the spatial control of the behavior of cells. (80) The production of silk micro- and nanoparticles can be accomplished using a number of different methods, including freeze-drying, grinding, spray-drying, jet-breaking, self-assembly, and freeze-thawing. (101-105)

Another technique that creates silk particles straight from fibers without the use of chemicals is milling silk fiber. By enhancing mechanical characteristics and cellular results, these particles are employed in drug carrier applications and scaffold reinforcement. (106) The difficulty in using the milling process is in obtaining uniformly fine silk particles. (10)

Proteins can be micropatterned onto substrates using conventional lithography methods as electron-beam lithography, soft lithography (SL), scanning probe lithography, and ultraviolet lithography (UVL). (107) SL is a quick, easy, and affordable method for patterning intricate molecular configurations important to biological applications and for manipulating surface molecular structures. Spin-coating RSF onto a silica substrate that has been subjected to argon fluoride excimer laser radiation is the procedure that is chosen to carry out UVL. (108) Inkjet printing is a method of micro-patterning that is both versatile and inexpensive, and it has the ability to limit incidents of cross-contamination while also accurately patterning intricate geometries. (107) Self-assembled peptide nanofibers have been patterned on RSF surfaces using inkjet printing to direct cell proliferation (80).

1.4.2.5. 3D Bioprinting Structures

Computer-aided design tools are utilized in the process of bioprinting, which is a technology that allows for the creation of intricate, high-definition materials. Due to the incorporation of architectural, biological, and mechanical signals, 3D bioprinting offers advantages over traditional TE. It can tune cell-cell junction stability, body shape, and alignment to create functional 3D tissue structures. (80) Biological inks (bioinks) are essential in 3D bioprinting technology, as they determine the structure and function of tissues. (109) Despite its application in TE, challenges remain, such as limited materials and cell type choices. (110) RSF is a unique material for 3D printing due to its biocompatibility and polymorphic nature. RSF can be printed via inkjet printing to create "nest" shapes. 3D printed RSF scaffolds can be regulated to form mesostructures and nanostructures by applying different mechanical stresses and dopants. (80) Recent research has shown that RSF can be chemically modified with glycidyl methacrylate to form a printable bioink (silk methacrylate) that can be printed to form complex structures, such as those in the brain and ear, using a digital light-processing 3D printer. (80)

1.4.2.6. Sponges

Sponges are porous structures that replicate physiological conditions. Their three-dimensionally porous structure promotes the adhesion, migration, and proliferation of cells as well as the diffusion or perfusion of nutrients and waste products in a static environment. (80) Their porous structure can be produced via gas foaming techniques, freeze-drying, and porogens. (111) By using alternative solvents for the regeneration of SF, such as aqueous solutions or organic solvents like 1,1,1,3,3,3-hexa-fluoro isopropanol (HFIP), processing parameters can be changed. (112) Porogens like sodium chloride (NaCl) are added to SF solutions that are cast into Teflon disk-shaped molds. This produces a highly homogeneous uniform pore size distribution. After air drying, the porous silk scaffolds are put in a vacuum dryer for a whole day. (113) As long as the size distribution of the sodium chloride particles is homogeneous, this technique produces RSF sponge scaffolds with a highly homogeneous uniform pore size distribution. Pore size can also be controlled by freeze-drying, which is determined by pH, fibroin content, and freeze-drying temperature. (114) Porous sponge structures can also be created via gas foaming, which is the process of adding ammonium bicarbonate to fibroin solutions. Because of its superior porosity and pore size control, RSF sponges are frequently utilized in tissue engineering, especially in bone and cartilage replacement.

1.5. Therapeutic Applications of Silk Protein in Cancer Research

2D cell cultures provide a number of benefits, such as being straightforward, affordable, and convenient for carrying out functional tests. Still, these systems have several significant drawbacks. (115) They are unable to mimic the intricate architecture of genuine tissues or tumors, which is essential for controlling drug metabolism, cellular differentiation, proliferation, viability, gene and protein expression, and other biological processes. (116-119) Significant changes in cellular morphology occur upon isolation and adaption to 2D environments. These changes result in a reduction of phenotypic variety and impact many functional characteristics, organizational structures, secretion profiles, and signaling pathways. (102-125) Moreover, alterations in contacts with the extracellular environment that result in the disruption of cell polarity impair the cells' ability to respond to a variety of stimuli, including apoptotic signals. (126-128)

Adherent cells' free access to vital elements like oxygen, nutrients, metabolites, and signaling molecules is another significant drawback of 2D culture techniques. (116) This is in contrast to the in vivo tumor environment, where a more varied distribution of these components is produced by the inherent architecture of the tumor mass. Thus, cellular gene expression, splicing patterns, architecture, and metabolic activities are all modified by the 2D culture environment. Furthermore, the majority of 2D adherent cultures are monocultures, which make it possible to examine a single cell type. The tumor

microenvironment and the niches needed by cancer-initiating cells are not replicated by this monoculture setting.

Furthermore, in light of these disadvantages, there is an urgent need for alternative models, such as 3D culture methods, which more closely match the actual microenvironment of the tumor. (115) These 3D systems provide a more physiologically relevant environment for understanding cancer biology and evaluating treatment choices. They do this by more closely imitating the conditions that exist in vivo for tumor masses.

3D tumor models have been developed as a result of advancements in cancer treatment. These models can be used to investigate cancer cell differentiation, proliferation, angiogenesis, drug resistance, immunosurveillance, and the testing of new treatments. (129,130) As a result of their proliferation in a microenvironment that is rich in nutrients and oxygen, these models are able to more accurately simulate in vivo cancer tissues than 2D monolayer cultures. A porous 3D scaffold for tumor cells is used for allowing mechanical integrity and hydration space for nutrients and metabolites to diffuse into the cells. Compared to 2D cultures, 3D cancer cell cultures show improved phenotype, changed gene expression, increased proliferation rate, glucose consumption, lactate dehydrogenase, and matrix metalloproteinase 9 activity. (131-134) They also show higher drug resistance, making drug testing more efficient due to their greater resemblance to in vivo tumors (see *Figure 4*). (132,135)

To be able to mimic this 3D environment, biomaterials such as alginate, chitosan, SF, agarose, and fibrinogen are used for developing bioengineered platforms. SF is one of the most used biomaterials for 3D tumor models because it is biocompatible, biodegradable, nontoxic, and induce only a mild immune response. Their exceptional mechanical properties, compatibility with common sterilization techniques, and simple preparation methods make them ideal biopolymers for cancer therapy. At the same time, silk-based formulations can be tailored for size, stability, drug loading, and release kinetics, accordingly. Considering all these advantages, scaffold-based systems based on silk fibroin are becoming more and more significant. In this field, research efforts are stepping up to create more accurate and efficient systems.

1.6. 3D Cell Culture Based Methods

Comparing standard 2D cultures to more physiologically realistic models produced by 3D cell culture techniques has changed research on cancer. The scaffold-based 3D culture systems, hybrid models, anchorage-independent, non-scaffold, and scaffold-based approaches are the main categories into which these methods fall. Each has unique benefits and drawbacks. To choose the best 3D cell culture model for a certain application in cancer research, it is essential to comprehend these attributes.

1.6.1. Non-Scaffold Based (Anchorage Independent)

In scaffold-free 3D culture techniques, cells self-aggregate in specialized plates such micropatterned plates that support microfluidic cell culture, low adhesion plates with ultra-low attachment coating, and hanging drop microplates. (136) Spheroids, especially the multicellular kind, allow for natural interactions between cells and also mimic the physiological features of tissues and malignancies in terms of cell-cell contact. (137) The size of a sphere is determined by the initial number of cells sown; it can be enlarged to a size at which tissue-like gradients of oxygen and nutrients are visible. Neurospheres are spheres made of mixed cultures of progenitor, glial, and neuronal cells. (138) They facilitate interactions between various CNS cell types and are crucial for neuronal differentiation, the transformation of toxic substances into active metabolites, and the release of apoptotic factors in response to medication. (139)

A range of tumor forms have been represented using tumor spheroid models that are either generated from pre-existing cell lines or acquired via ex vivo propagation of tumors from individual patients (tumor organoids). Patient-derived tumor spheroids are valuable tools for patient-centered therapy development and drug screening since they preserve their genome across time (140). Spheroids are more reproducible when they are uniform and of a size that prevents necrosis and inadequate food delivery, although this is a drawback of spheroid cultures. This requires extensive culture environment modification. (136)

1.6.1.1. Hanging Drop Microplates:

This technique suspends cells in tiny droplets of fluid, which promotes cell aggregation into spheroids. It was possible to study nutritional gradients and waste accumulation because the spheroids created tissue layers that mimicked one another and had discrete proliferative, quiescent, and necrotic zones. bigger spheres might need to be transferred to plates with bigger medium volumes because sphere size is determined by the original number of cells. Applications include the building of cardiac spheroids utilizing iPSC-derived cardiomyocytes, endothelial cells, and fibroblasts to investigate heart tissue, as well as cancer research and toxicity testing in hepatocytes. (136)

1.6.1.2. Spheroid Microplates with Ultra-Low Attachment Coating (Low Adhesion Plates):

Spheroid microplates with rounded, tapered, or V-shaped bottoms work similarly to hanging drop plates (HDP) cultures in that they use the absence of cell attachment sites to encourage cell aggregation and spheroid formation. However, unlike HDP cultures, spheroids can frequently be cultured for longer periods of time without needing to be transferred to a new plate for experimental purposes. (136) Polystyrene is frequently used to create low adhesion plates, which are then coated with hydrophilic or hydrophobic materials like agarose (141) or the non-adherent polymer poly hydroxyethyl methacrylate (HEMA). (142)

The material poly-HEMA encourage cell aggregation into spheroids without requiring translocation. They are widely utilized in tumor studies and are appropriate for multicellular cultures. Examples include the formation of brain tumor spheres for drug delivery evaluations and non-small cell lung cancer spheres with stem-cell-like characteristics. The plates facilitate the investigation of drug resistance, hypoxia, and dormancy, among other in vivo tumor properties. (136)

1.6.1.3. Magnetic Levitation

This novel method includes preloading cells with magnetic nanoparticles, which cause the cells to float and aggregate into spheroids when exposed to a magnetic field. (136) It has been applied to TE, mesenchymal stem cell spheroids, and a variety of tissues. This method of creating glioblastoma spheroids closely resembles in vivo protein expression. (143) In order to improve drug discovery, magnetic levitation has potential for high-throughput toxicity screening in 3D cultures. (144)

1.6.2. Scaffold Based (Anchorage Dependent)

In order to replicate the ECM, scaffold-based 3D cell culture techniques provide physical support for cell aggregation, proliferation, and migration. (136) These scaffolds can be synthetic or biological, and based on their chemical and physical qualities, they each affect the characteristics of cells.

1.6.2.1. Polymer-based Scaffolds

Polymer-based scaffolds are a potentially game-changing instrument for 3D cell culture because of their capacity to imitate the ECM that occurs naturally and to offer a biomimetic environment that encourages cell proliferation and differentiation. This scaffold has a great deal of potential for use in cancer research because of its capacity to offer a versatile platform for the investigation of complex cellular functions.

Table 1: Properties comparison of 2D and 3D cell culture-based methods, recreated from Kapałczyńska M. et all. (115)

Properties	2D	3D
Time for formation	Within minutes to a few hours	From a few hours to a few days
Culture quality	High reproducibility, long-term culture, easy to interpret, simplicity of culture	Low reproducibility, difficult to interpret, cultures more difficult to carry out
In vivo imitation	Do not mimic the natural structure of the tissue or tumour mass	In vivo tissues and organs are in 3D form
Cell interactions	Deprived of cell-cell and cell-extracellular environment interactions	Proper interactions of cell-cell and cell-extracellular environment
Characteristics of cells	Changed morphology and way of divisions; loss of diverse phenotype and polarity	Preserved morphology and way of divisions, diverse phenotype and polarity
Access to essential compounds	Unlimited access to oxygen, nutrients, metabolites and signalling molecules	Variable access to oxygen, nutrients, metabolites and signalling molecules
Molecular mechanisms	Changes in gene expression, mRNA splicing, topology and biochemistry of cells	Expression of genes, splicing, topology and biochemistry of cells as in vivo
Cost of maintaining the culture	Cheap, commercially available tests and the media	More expensive, more time-consuming, fewer commercially available tests

They are classified as belonging to both the natural and the synthetically manufactured categories. (145)

These natural polymers are utilized in the production of natural polymer scaffolds. Natural polymers can be processed into a range of morphologies, including fibers, films, or porous structures, before being used. Skeletons that are based on proteins and scaffolds that are based on polysaccharides are two primary categories that can be further subdivided. (145) Examples of large molecules that are composed of amino acids include collagen, silk, gelatin, and fibronectin. These structures have the potential to regulate the creation of tissues and the adherence of cells, in addition to acting as sources of protein-based scaffolds. (146,147) Polysaccharide-based scaffolds, on the other hand, are composed of long chains of sugar molecules composed of hyaluronic acid and chitosan. It is common practice to modify the physical and biological features of these scaffolds, and they are biocompatible and biodegradable. (145)

The mechanical and biochemical properties of synthetic polymer scaffolds, including as polylactic acid, polyglycolic acid, and polycaprolactone, can be engineered to meet specific needs; however, surface modifications could be necessary to encourage cell adhesion and growth. (148) Natural polymer scaffolds can be used to build 3D cell culture models for cancer research that are more physiologically accurate, which could result in the development of more potent treatment approaches. (145)

1.6.2.2. Hydrogel Scaffolds

With their ability to absorb substantial volumes of water or biological fluids without compromising their structural integrity, hydrogels are 3D networks composed of hydrophilic polymers (149). The dome approach, insert wells technique, gel-bottom support method, and embedding technique are just a few of the methods that can be applied to these hydrogels. To seed cells as droplets inside a cell culture vessel, the dome technique combines cells with hydrogels that are sensitive to temperature. For the hydrogel to polymerize and form a dome structure, this method depends on precise temperature control. (145)

Cell culture media is added to the well around the porous inserts, which are used in the insert wells approach to contain the cell-hydrogel mixture. Because of this separation, a new environment is created inside the insert that permits nutrient exchange while preserving the insert's unique 3D culture. Eventually, the insert bottom will form heterogeneous spheroids as a result of cell-to-cell contact and gravitational force. By applying chemo attractants on one side of a permeable membrane and the cell-hydrogel mixture on the other, this technique can be utilized to analyze cell invasion or migration. (145)

Using the gel-bottom support approach, the cell suspension is layered on top of a thick layer of hydrogel that has been created at the bottom of a culture well. This technique is useful for researching drug reactions, invasion, migration, and interactions between cells and cells in a matrix. Evenly embedding cells in the hydrogel and removing them for further investigation from the matrix can be more technically difficult. (145)

Since polyvalent hyaluronic acid (HA) hydrogels are usually made by chemically modifying HA molecules to include crosslinking agents or functional groups that facilitate the creation of a gel-like structure, they are regarded as synthetic. By varying the proportion of aldehyde-HA in the hydrogel formulation, the created HA hydrogels' qualities may be modified to better mimic the topography and mechanical attributes of breast cancers. The capacity to adjust the mechanical characteristics of the hydrogels creates opportunities for simulating various tumor kinds or phases of tumor development. (145)

Gelatin methacryloyl (GelMA), a natural biomaterial used for 3D hydrogel scaffolds in cancer research, is derived from gelatin and modified to undergo photo crosslinking when exposed to ultraviolet light. GelMA hydrogels have tunable mechanical and biochemical properties, biocompatibility, and support cell growth, making them valuable tools for studying cancer cell behavior, invasion, drug screening, and other aspects of cancer research. (145)

1.6.2.3. Decellularized Tissue Scaffolds

Decellularized tissues—that is, tissues devoid of all cellular components—can be 3D scaffolds for cell culture. All vital for tissue organization and cell function, growth factors, signaling molecules, and structural proteins still abound in these tissues coupled with their complex ECM composition. This then affects the adhesion, motility, invasion, and differentiation of the cancer cells by allowing more near contacts between them and the extracellular matrix. By means of decellularized tissues, which offer spatial order and architectural cues influencing cellular behavior, one can also investigate angiogenesis and vascularization processes in the evolution of cancer. (145)

Decellularization methods including chemical, physical, and enzymatic processes are used to remove cellular elements without compromising the integrity of the extracellular matrix. The decision relies on the type of tissue, the scaffold's characteristics, and the study's requirements as well as the best results may come from mixtures of techniques. Challenges include immunogenicity and biocompatibility, process standardizing and repeatability, and integration with innovative technologies as microfluidics or organ-on- a-chip systems. These components ensure that studies complement one another and simplify comparison of results. (145)

Furthermore, influencing cellular mechanotransduction and hence gene expression patterns, cell shape, and proliferation are mechanical stiffness and support they provide. Decellularized tissue scaffolds can be produced using several sources, including specific tissue compartments or solid organs. Still, there are problems in the field including immunogenicity and biocompatibility, repeatability and standardizing of decellularization techniques, and integration with modern technologies. Decellularized tissue scaffolds also provide a suitable platform for investigating the interactions between two often seen components of the ECM: endothelial cells and macrophages. These cells are well-known for their contribution to the spread of cancer in solid tumors; as decellularized matrices closely reflect the surroundings seen in tumors naturally, they are a perfect instrument for investigating these interactions. (145)

1.6.2.4. Hybrid Scaffolds

Through the utilization of a wide range of scaffold types inside 3D cell culture systems, it is possible to generate models that closely resemble the physiological circumstances that are present in actual tissues. This has the potential to assist researchers in constructing models that are more accurate for the purpose of understanding the progression of disease, cellular activity, and therapeutic responses. This method makes use of a combination of synthetic and natural polymers, also known as hydrogels, and provides a variety of mechanical, chemical, and physical cues that have a significant influence on the behavior of cells. The combination of scaffolds has the potential to improve the functionality of these systems by several means, including the incorporation of specialized characteristics, the incorporation of microvascular networks, and the exact release of growth factors. The application of this method has the potential to significantly improve our comprehension of tissue biology as well as the fundamental components that are responsible for the development of illnesses. (145)

1.6.3. Specialized 3D Culture Platforms

1.6.3.1. Microfluidics

Microfluidic devices, which are designed for use in perfusion-cultured cell cultures, let nutrients and oxygen be delivered continuously while simultaneously removing waste. These shear forces are detected in living cells, such as endothelial cells, when they are subjected to blood flow. It is possible to develop microfluidic devices that can reproduce these shear forces. In addition to being a component of the device itself, a physical barrier that serves to divide the compartments may also take the form of a non-physical barrier, such as a supporting matrix that mimics the ECM. Utilizing microfluidic devices allows for the continuous application of drugs or other soluble compounds, such as growth factors. Furthermore, they can be employed to aid in the movement of liquid between multiple compartments that may consist of different types of cells. (136) Various organs, such as skin, muscle, liver, and neural tissue, have been extensively studied using three-dimensional tissue models. These models were developed by establishing a link between cell culture in a lab setting and animal models in a real-life environment. By utilizing microengineering techniques, it becomes feasible to create platforms that integrate organs on a chip. In the future, with the progress of 3D culturing methods, organs-on-a-chip will offer state-of-the-art tools for high-throughput screening and medication development. (150)

1.6.3.2. Organoids

The term "organoids" was initially used to describe primary tissue cultures that were isolated from the stroma in 3D gels. However, the term has now been expanded to include self-renewing and self-organizing 3D cultures that are composed of primary tissue, embryonic stem cells, or induced pluripotent stem cells. (151) As a result of a number of factors, including the lack of a local microenvironment and interactions with immune cells, these cultures are not ideal for the purpose of imitating immunological reactions. On the contrary, organoids that are derived from human cells have the potential to provide nearly physiological models for the purpose of studying human diseases and development. In addition to being more affordable than using animal models for drug discovery, advanced organoid cultures can be utilized to create accurate models of human diseases that are impossible to replicate in animals. (135) Numerous organs, including the brain, kidney, lung, prostate, and digestive tract, have been described as organoids. (152) Organoids are frequently used downstream for transcriptome profiling, but their uses in precision medicine and drug development are growing. (153) Furthermore, tumoroids made from cancer patient tissues can offer sophisticated 3D culture platforms for the development and assessment of customized drugs. (154)

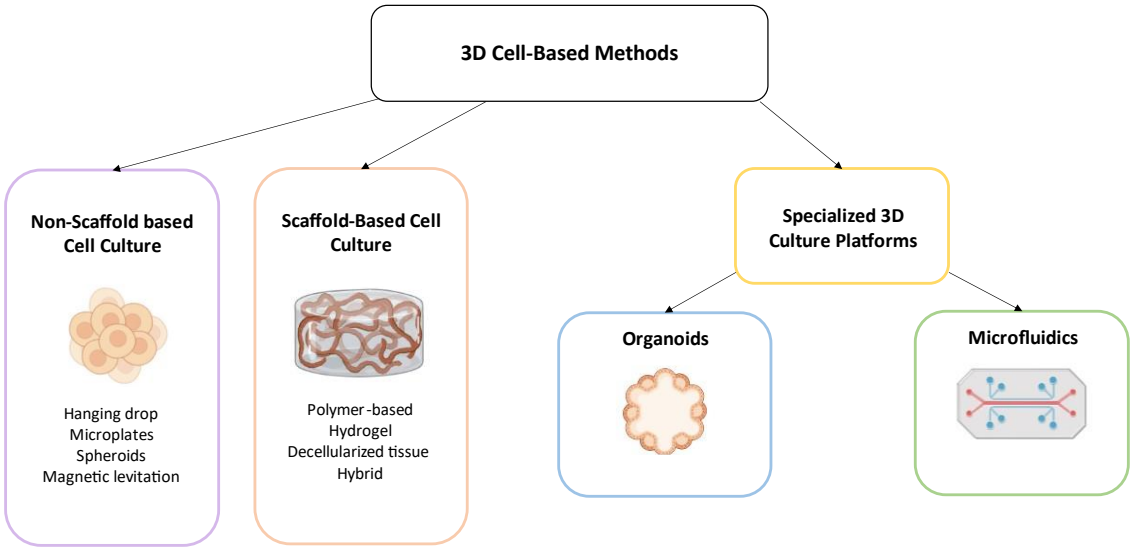

Figure 4: 3D Cell-based methods take shape under 3 main groups. They are summarized as non-scaffold based and scaffold-based cell culture as well as specialized 3D culture platforms. Generated by BioRender.

Aim of the Master Thesis

The silk sponges, have the potential to promote high-throughput experimentation. Usage of silk sponges enables researchers to explore many aspects of cancer, ranging from the assessment of drug efficacy to the exploration of novel therapeutic treatments. This cutting-edge method not only simplifies the research procedure, but it also offers a versatile and dependable instrument that can be used to investigate the complexity of cancer in a manner that is more regulated and reproducible.

To able to have a successful evaluation, it is of utmost importance to first optimize the silk sponges to be used. In order to select the optimized sponge, the steps in the development of a silk sponge should be considered, and it must be realized that silk sponge production involves several critical steps (see *Figure 5*). These important stages can be briefly summarized as follows: cocoon cleaning and sericin protein removal from silk using Na_2CO_3, dissolving and dialyzing, lyophilization and sponge casting. Throughout this process, some parameters are not precisely defined. These mentioned parameters are the amount of methanol used and the incubation time of methanol, bed height and silk solution ratio.

Definition of these steps is critical during sponge production because these steps are thought to cause changes in various properties of the sponge. In order to achieve this, more than one silk sponge should be cast and a comparison should be made. To enable this comparison, silk sponges need to undergo a series of assessments.

In this master thesis, research has been carried out to optimize and characterize silk sponges. The methods used for this purpose are summarized in *Table 2*. This study will use various analytical techniques to thoroughly investigate and characterize materials. Visual testing assesses structural integrity and strength, while IR measurements provide information about molecular composition. Protein analysis, using techniques like SDS-PAGE and Western blot, focuses on understanding the protein composition of materials, providing crucial data for biomedical applications. CD measurements study secondary protein structure, while SEM provides high-resolution images of surface morphology. Porosity and density assessments help us to understand internal structure, while water retention, swelling ratio and water-uptake capacity is provide insights into hydration behavior. Degradation of silk

fibroin is carried out by enzymatic digestion using the enzymes α-chymotrypsin and protease. These techniques form a robust methodology for comprehensive characterization, enabling a thorough evaluation of materials' mechanical, chemical, and structural properties.

The study also includes assessing potential toxicity of materials through period leaching, stress testing, and leaching in organic solvents based on HT-29 cell line. The HT-29 human colon cancer cell line is a crucial tool in biological and cancer research, contributing valuable insights for improved diagnostics, treatment strategies, and a more effective approach to combating this significant public health concern. Its use in research endeavors reflect its significance in understanding colorectal cancer based on in vitro assessments.

The MTT (3-(4,5-dimethylthiazol-2-yl)-2,5-diphenyltetrazolium bromide) assay will be used in a high-throughput 96-well plate format to simulate prolonged exposure, and leaching in organic solvents. The 96-well plate format enhances efficiency, allowing simultaneous screening of multiple conditions. This multidimensional approach aims to uncover insights into material safety, paving the way for informed advancements in materials science and application.

The outcomes of this work include the optimization of scaffold-based investigations using silk sponges to improve the accuracy and consistency of colon cancer research as well as creation of a standardized production process for scaffolds, contributing to the reproducibility and scalability of the methodology. Via this research it is aimed to reduce reliance on animal testing in preclinical studies, enhances our understanding of colon cancer, and aligns with ethical considerations. This move is a significant step forward in fostering innovation and prioritizing the ethical treatment of living beings in biomedical research. The automatized system will improve accuracy and predictive value, mirroring in vivo conditions.

Table 2: Methods used in the evaluation of silk sponges and evaluated properties

Method	Evaluation
Visual testing	Structural integrity and strength
Scanning electron microscopy (SEM)	Surface morphology
Water retention, swelling ratio and water uptake	Hydration behavior
Fourier transform infrared spectroscopy (FTIR)	Molecular composition
SDS PAGE & Western blot	Protein analysis
CD measurement	Secondary protein structure
Enzymatic digestion	Degradation of silk fibroin
MTT	Cell viability

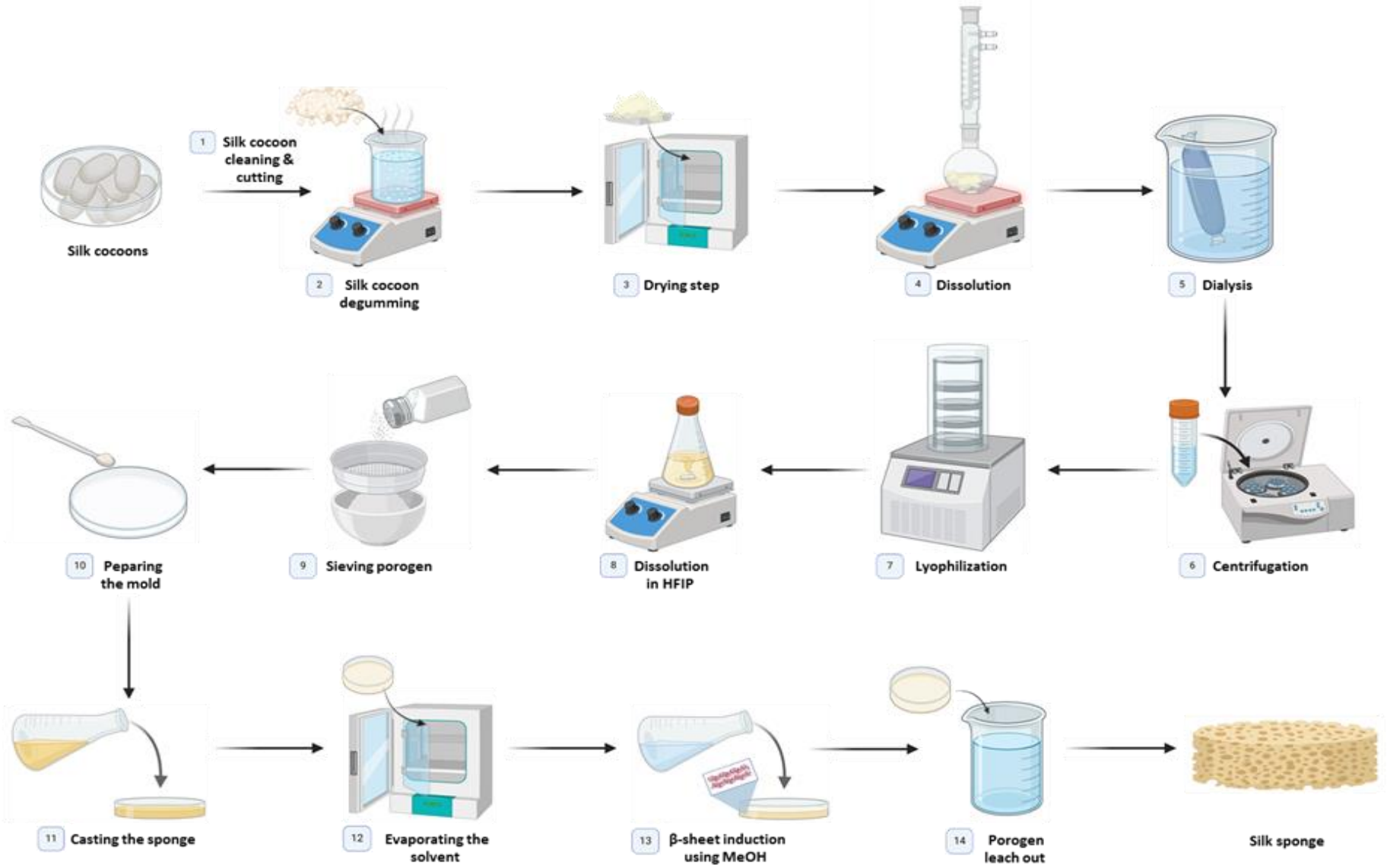

Figure 5: Silk sponge production steps include several essential steps that start from the cleaning & cutting of silk cocoon to casted silk sponge. Created by BioRender.

2. Materials and Methods

2.1. Materials

Silkworm cocoons of *Bombyx mori L.* were acquired from the Sericulture and Agriculture Experimental Station (Vratsa, Bulgaria), sodium carbonate from VWR International (Radnor, USA) ethanol 96% from Merck (Darmstadt, Germany), dialysis tubes from Spectra/Por from Spectrum™ Labs (Irving, USA), and methanol and NaCl from VWR International (Radnor, USA), The Revert 700 total protein stain was obtained from Li-Cor (Lincoln, USA) and the chemicals used for the protein analysis were purchased from Bio-Rad (Hercules, USA). All other reagents were acquired from Sigma Aldrich (St. Louis, USA) and utilized precisely as they were received including Trypsin/EDTA (1x), thiazolyl blue tetrazolium bromide, Dulbecco's phosphate-buffered saline (PBS), and Roswell Park Memorial Institute-1640 (RPMI-1640). The biopsy punchers were purchased from pfmmedical (Cologne, Germany).

2.2. Methods

2.2.1. Production Silk Sponges

2.2.1.1. *Cocoon Cleaning*

Bombyx mori L. silkworm cocoons were cut open innermost layer, and the dried silkworm were removed. Then the sericin was removed by following steps. 1.6 L of deionized water was added to a 2 L glass beaker and covered with aluminum foil. The beaker was placed on a heating plate and set to approximately 300°C. The continuous stirring was applied to the beaker by using magnetic stirrer. 3.4 g Na_2CO_3 was added to the water at 50-60°C and 4 g cleaned cocoons were added once the solution started to boil. The cocoons had to be stirred with a glass rod every ten minutes while they were boiling for 30 min. After the sericin removal process, the degummed silk was washed with tap water multiple times. Excessive water was gently removed and the fibroin strands were arranged on aluminum foil and placed in the incubator at 50°C till they were completely dry.

2.2.1.2. *Dissolution and Dialysis*

For the preparation of the silk solution, the completely dried, degummed silk was dissolved in a mixture of $CaCl_2$, 96% ethanol and distilled water in the ratio of 1:2:8, considering that there should be 10 times more solution than the amount of silk. The calculated amount according to the silk mass. of $CaCl_2$ was then dissolved under stirring in the round bottom flask with a condenser and heated up until the solution was refluxing. Then the dried and degummed silk was added piece by piece. After the silk addition, the mixture needed to boil for another 45 min. During the boiling time the dialysis step was prepared. Cellulose dialysis tubes with a molecular cut-off of 6-8 kDa were pre-soaked using tap water. One end of the tube was closed using clips before the solution was added. The upper part was closed without leaving any air bubbles in the tube. The tubes were then put to dialysis in a beaker filled with distilled water for 3 days. During this period, water was renewed every day. The solutions were put into centrifuge tubes, and they were centrifuged at a speed of 3200 rpm per minute for ten minutes. The silk solution was stored in the freezer at a temperature of -20°C prior to lyophilization.

2.2.1.3. Lyophilization

The silk sponges lyophilization process of was accomplished with the help of a Christ Alpha 2-4 LD Plus lyophilizer (Christ MartinTM, VACUUBRAND). The vacuum pump was heated up for twenty minutes, and the machine was started by following the manufacturer's instructions. The samples of frozen silk placed in a flask with a round bottom and attached to the lyophilizer. The lyophilization process lasts for approximately one day.

2.2.1.4. Sponge Casting

To prepare a silk solution, lyophilized silk was dissolved in HFIP purchased from Sigma Aldrich (St. Louis, USA), resulting in 16% (w/v) silk concentration. The porogen (NaCl) was sieved and the fraction of 500-800 µm was selected. A 10 cm diameter petri dish was filled with porogen and the surface was flattened. Then approximately 25.5 ml solution were poured on top and let infiltrate into the salt bed. The petri dish was then incubated at 50°C for one hour covered with the lid and afterwards uncovered until it was completely dry. The β-sheet structure was induced by incubating the dry silk-salt-piece in 90% methanol for 1 h. The porogen was removed by immersing the petri dish in distilled water, changing the water twice a day for two days, and carefully removing the sponges from the molds. The sponges were stored in 70% ethanol as a sterilizing step and for long time storage.

2.2.2. Visual Testing

Visual examination of the test object under normal lighting conditions and with a microscope was performed. Some of the visual indicators of probable flaws that were investigated for included surface cracks, corrosion, weld discontinuities, surface finish concerns, dimensional mistakes, and other visual elements.

2.2.3. Scanning Electron Microscopy (SEM)

The sponge samples were cut into 2×2×3 mm pieces. During this process, great care was taken during the cutting process in order to not disrupt the integrity of the structure. Using a sputter coater, scaffolds were coated with a 5 nm coating of gold particles before imaging. Quorum Q150R ES machine from Quorum Technologies Ltd. (East Grinstead, UK) was run on 120 s at 50 mA and the coating was performed using argon. The surface and cross-section morphologies of the scaffolds and pore distributions, sizes, and interconnectivity were observed with JEOL JSM-6510 SEM from JEOL GmbH (Eching/Munich, Germany). Images were taken through JEOL Scanning Electron Microscope Program, using backscattered electrons at an accelerating voltage of 5 kV. Scaffolds were scanned at x50 magnitudes to show morphology and pore structure.

2.2.4. Water Retention, Swelling Ratio and Water Uptake

With the help of a 6 mm biopsy puncher, the SF sponges were sliced into pieces, and then stored in Eppendorf tubes. Due to the fact that the samples were kept in ethanol at a concentration of 70%, distilled water was added multiple times in order to eliminate the ethanol, and then the samples were left on the shaker. This procedure was carried out for a period of two days, during which time the distilled water was frequently replaced at regular hourly intervals. Before the sponges placed into the incubator, their wet weight was measured as “Ws”. Excess water was removed by touching the edge of the Eppendorf tubes with biopsy puncher before wet weights were determined. The measurement method was conducted at time points 1, 2, 4, 8, 24, 28, and 48 h using a highly accurate scale from VWR International (Radnor, USA). The 1 h measurement was set to W. This measurement was repeated 3 times by taking 3 samples from each sponge. The samples were observed to be completely dried at 24 h each time and the 24 h measurement was determined as Wd. Water retention was determined as a percentage by the formula below:

$$Water\ retention = (\mathrm{Ws} - \mathrm{W})/(\mathrm{Wd} * 24\ \mathrm{h}) * 100\%$$

Equation 1: Water Retention

Swelling ratio was calculated with the following formula:

$$Swelling\ ratio = (Ws - Wd)/Wd$$

Equation 2: Swelling Ratio

And water uptake values were calculated as percentages with the formula below:

$$Water\ uptake = (Ws - Wd)/Ws * 100\%$$

Equation 3: Water Uptake

2.2.5. Fourier-Transform Infrared Spectroscopy (FTIR)

The SF sponges were cut into pieces with a biopsy puncher. The samples were prepared for IR spectroscopy by adding 1 ml of 70% EtOH in Eppendorf tubes. Values were obtained using the Platinum-ATR alpha machine from Bruker (Billerica, USA). To obtain information about the molecular structure of the silk, 4 cm^{-1} resolution IR spectra were recorded in the scan range of 400 to 4000 cm^{-1}. Before starting the measurement of the samples, the background was measured. Samples (n=30) were placed vertically for spectroscopy. The secondary structure of silk was quantified mainly by examining the ß-sheet structure, with the assistance of OPUS software.

2.2.6. Protein Analysis

2.2.6.1. SDS-PAGE & Western Blot

The SDS-PAGE process involved assembling Mini-PROTEAN TGX pre-casted gradient gels 4-20 % 10 well for 30 µl and an electrophoresis chamber, filling it with a 1x electrophoresis buffer, and washing the wells with a buffer. The pipette will be sampled and blanked into the wells, avoiding air bubbles and overflowing into neighboring wells.

The silk samples that underwent treatment were dried in the oven at a temperature of 70°C for the duration of one night. A 1% silk solution was created by dissolving silk punch in the necessary amount of 9 M lithium bromide solution acquired from Sigma Aldrich (St. Louis, USA). The dissolution process took place in an incubator at a constant temperature of 50 °C for 24 hours. Subsequently, the 1% silk solution underwent dialysis in pre-soaked dialysis tubes overnight, with water being changed twice. The samples were subjected to heat and vacuum reduction using a rotation-vacuum concentrator ALPHA RVC from Christ (Osterrode am Harz, Germany) until a protein concentration of 0.8 µg/µl was achieved. The protein content was quantified using a nano spectrophotometer from IMPLEN (Munich, Germany) by the Bradford test.

10 different samples were seeded to the wells including the blanks and ladder. 3 parts reduced sample and 1 part protein dye were heated to 90 °C for 5 minutes in order to prepare the SDS-PAGE. 15 µl of distilled water, 5 µl of protein dye, and 2 µl of a pre-stained protein ladder were prepared and handled similarly to a protein sample as a reference. The samples were placed into the gel pockets at an amount of 20 µl. The chamber was closed, and the lid was connected to the power supply, starting at 60 V. The voltage was increased to 80, 100, and 120 V through 20-min time periods. When the dye front reaches the end of the gel, the electrophoresis process is terminated without further action. The nitrocellulose membrane was activated when the loading dye front reaches the last 1.5 cm of the gel by washing with distilled water for 20 min.

The sandwich blot was prepared as follows: black plate, a single fiber pad, two Whatman papers (filters), the SDS-PAGE gel, the activated nitrocellulose membrane, two further Whatman papers (filters), a second fiber pad, and ultimately a transparent plate. In order to remove any air bubbles that may have become trapped, the stack was gently rolled over. After the blotting cassette has been sealed, it has been inserted into the chamber. After inserting an ice pack, the chamber was filled to the brim with Harlow buffer until the indicator that reads "Blotting" or "4 gels" appears on the screen. The electrophoresis was performed for a duration of 1 h while maintaining a current of 350 mA.

After this procedure, the single-color Western blot process was performed to detect and visualize all proteins. Methanol was added to the stain reagent as indicated on each bottle. Then the membrane

was rinsed with water and incubated in 5 ml of Revert 700 Total Protein Stain solution for 5 minutes, with gentle shaking. Afterwards, The Total Protein Stain Solution was decanted. The membrane was rinsed 2× for 30 sec with approximately 5 ml of Wash Solution that contains 6.7% (v/v) Glacial Acetic Acid, 30% (v/v) Methanol in water. After completing the rising process, the membrane was directly imaged with Li-Cor Odyssey Imaging System (Lincoln, USA) and Li-Cor Image software in the 700 nm channel.

2.2.6.2. CD Measurement

The CD was measured in or near the absorption bands of the silk protein, which is particularly valuable for assessing the secondary structure elements such as alpha helices, beta sheets, and random coils. Quartz cuvettes with a path length of 1 mm were cleaned carefully before usage. Samples were prepared by vortexing the protein solution that is prepared as the same way with the samples of SDS PAGE to obtain a homogeneous solution. 938 µl of distilled water and 62 µl of protein solution were added into Eppendorf tubes and vortexed intensively.

Chirascan Plus machine from Applied Photophysics Ltd. (Leatherhead, UK) with its software ANM System 2.0.2 for nitrogen supply and its controlling software Pro-Data Chirascan was used for CD measurement. The nitrogen levels were checked and the 'active management nitrogen system' was started. After opening the application, 'start lamp Ignite Sequence' was selected. Curve detection was done by Chirascan. The lamp needs to be equilibrated before usage. First, the water was tried out as a blank to detect. The spectra of a silk fibroin solution containing 50 µg/ml were determined. Every sample had its CD spectra recorded between 190 and 280 nm at 22 °C and 1-3 l/min of N_2 flow. Every spectrum was measured with a resolution of 1 nm, and the averages of five consecutive scans were shown. The sample values were removed to derive the blank value. To guarantee that each sample cell was clean, it was cleansed using ethanol and distilled water before usage. The sample-filled cuvette was visually checked for bubbles, particles, and blurring to avoid interferences.

2.2.7. Enzymatic Digestion

Using a biopsy puncher, 3 samples were taken into separate Eppendorf tubes. One of the samples was treated with 100 µl of protease from Streptomyces griseus (Sigma Aldrih, 9036-06-0) and 900 µl of PBS. The second sample was treated with 100 µl of α-chymotrypsin from bovine pancreas (Sigma Aldrih, 9004-07-3) and 900 µl of PBS. The third sample was prepared for enzymatic digestion by adding 800 µl PBS to 100 µl protease and 100 µl α-chymotrypsin. Different enzyme concentrations of 0.25 mg/ml, 0.50 mg/ml and 1.00 mg/ml were used for digesting the silk sponge samples. Over a period of 7 days a daily replacement of the enzymatic reaction PBS was removed from the falcons and fresh solutions were added for degradation. To be able to obtain the visual results from the digested structures, the samples were prepared for SEM.

2.2.8. Cell Culture

HT-29, derived from the American Type Culture Collection, was the immortalized human colorectal adenocarcinoma cell line upon which all of the cell culture experiments carried out for this master project. Cells were grown in T75 flasks at 37°C with 5% CO_2 under standard cell culture conditions. RMPI-1640 media was fully supplemented with 10% fetal bovine serum (FBS), 1% penicillin (10,000 U/mL)-streptomycin (10,000 µg/mL) combination, and 1% L-glutamine (200 mM) in order to encourage cellular development and survival. To keep sterility and stop contamination, the next operations were carried out with great respect to aseptic methods. The methods were carefully carried out in sterile facilities such as laminar-flow hoods to guarantee the integrity of the experimental conditions and the accuracy of the research results.

2.2.8.1. Cell Splitting

To ascertain the rate of splitting, the confluence of the cells was examined under a microscope. Prior media was removed to facilitate cell splitting, followed by a 5 mL wash with Dulbecco's PBS. In order to separate the cells that were sticking to the flask, a solution of trypsin/EDTA 0.05% (1x) was added, and the mixture was allowed to incubate for 10 minutes. Following the addition and resuspension of 3 mL of fresh RPMI-1640. The cell- trypsin-media suspension was taken to 15 mL falcon tubes. 13 mL of fresh media was added.

The T75 flask was examined under microscope. Cell suspension was added when small number of cells were detected on the flask's surface. In cases where sufficient cells were found during the examination under microscope, the flask was sterilized by spraying with ethanol again and left to incubate. In the following days, the flask was regularly examined under a microscope and the cell growth process was checked. The splitting process was repeated in cases where the confluency exceeded the 80% limit.

2.2.8.2. Cell Counting

The cell suspension was resuspended and. 2 µl of cell suspension was transferred into a 1.5 ml Eppendorf tube. 98 µl of PBS was added to diluted cell suspension to a ratio of 1:50. 10 µl of diluted suspension was counted with a Neubauer cell counting chamber. The Neubauer counting chamber has two spots for application of the prepared cell suspension. Each spots measure 3×3 mm and consists of nine squares. Each square has 16 equal squares with 1×1 mm total size. Cells in four separate chambers were counted separately using a microscope. Cells on the window walls of two outer or two inner lines were not included in this calculation.

When all four individual chambers had been counted, cell concentration was calculated using the following equation:

$$cell\ concentration\ \left(\frac{cells}{mL}\right) = \frac{Total\ Counted\ cell\ number}{4} * 10000 * 50$$

Equation 4: Cell counting

2.2.8.3. MTT Assay for Sponge Leach out

The sponges were removed from the ethanolic suspension and the ethanol was replaced by fully supplemented RPMI media. Eight sponge samples were taken for the time points: 0,24,48,72,96,120,144, and 168h time. The old media was removed from the sponges via applying pressure on sponges with tweezers and with a help of pipette released old media was taken out one by one based on the time points. Sponge samples were placed in a 12-well plate (VWR® Tissue Culture Plate, USA) with 1 ml of fresh media. 96-well plates (VWR® Tissue Culture Plate, USA) were seeded with 2000 HT-29 cells/well, and the cells were allowed to settle and resume exponential growth before treatment. 100 µl of cell suspension per well was added. For each of the 8 time points, 6-fold technical replicate were cultured.

On the last day of the leaching period, the 0th hour sponge was treated with media while only soaking the sponge once. The old media was removed from the 96-well plate and 100 µl/well of the leachate media was added. The plates were incubated at 37°C for a 72 h. After the process, MTT Media- (RPMI1640 without supplements) the tetrazolium bromide solution (5mg per ml in PBS) was prepared in a 7:1 ratio. The leachate media was removed and replaced by 100 µl/well. MTT working solution and incubated by 37°C for 4 h. Afterwards, the MTT working solution was replaced by 100 µl of DMSO. 100 µl of DMSO was used as blank sample. The absorbance was measured at 560 nm with a reference of 650 nm wavelength value using a TECAN plate reader after 10 seconds of shaking. 6-wells of the 96 well plate was seeded for each timepoint and the three closest values were then chosen for study.

2.2.9. Statistical Analysis

The study utilized Microsoft Excel and GraphPad Prism for data analysis, identifying noteworthy trends and patterns. Statistical significance was determined using the one-way Analysis of Variance (ANOVA) test. As a normalization step to reduce any confounding effects, the mean value of DMSO was removed from the chosen values of the three wells after data gathering. In order to better understand the central tendency and variability of the recorded data points at each time point, calculations were performed on the resulting adjusted values of the three selected wells. This involved determining the mean and standard deviation. Normalization to the blank value (100%) was used to establish a baseline for making comparisons. This normalizing process enabled a standardized evaluation of cellular responses over time, allowing for the calculation of percentage values for each time point based on the initial experimental circumstances. The significance is defined as follows: * p-value less than or equal to 0.05, ** p-value less than or equal to 0.01, *** p-value less than or equal to 0.001, **** p-value less than or equal to 0.0001. All experiments were performed at least in three independent repetitions. Results were presented as mean ± standard deviation, with error bars in graphical representations.

3. Results and Discussion

3.1. Production of Silk Sponges

The silk production method was optimized by casting 30 distinct samples with varying bed heights, methanol incubation times, salt solutions, and methanol concentrations. This was done in order to achieve the best possible results in the process of fabricating silk sponges. In order to facilitate the conduct of characterization tests, these sponges have been represented by abbreviations. The characteristics of all samples are summarized in *Table 3*.

Since all samples were cast in wells with a diameter of 3.5 cm, the maximum salt bed height was determined as 1.4 cm. Because silk sponge integrity must be ensured, and in case of higher levels of porogen use, it should not overflow from the wells. Additional bed heights selected for a more accurate comparison are 1 cm and 1.2 cm After the bed height properties were decided, 3 different silk solution amounts were proceeded, namely 4, 4.5, and 5 ml.

Cast sponges have been analyzed in various groups to examine the bed height/silk solution ratio. Three samples (AD, AE, AF) were cast in a 1.4 cm bed height following 3 different silk solution amounts to be able to determine the best ratio. In the same way, 3 sponges with a bed height of 1.2 cm were casted (AA, AB, AC). Another group were sponges with a bed height of 1 cm with different silk solution amounts (D, E, F).

Other parameters that were tried during sponge casting were the amount of methanol and incubation time with methanol afterward. In order to observe the effects of incubation time on silk sponge production, two different times were determined. These times are 30 and 60 minutes. In this context, 6 sponges with 1 cm bed height and 4 ml silk solution were cast. 3 of them were incubated for 30 min (T, U, V) while the other 3 sponges were incubated for 60 min (W, X, Y). Both groups were administered 3, 3×2, 3×3 ml of methanol, respectively.

To ascertain the quantity of methanol, another batch of sponges were cast. The silk sponges were treated in the same amount as the silk solution, which is 5 ml (A, B, C) for 3 different bed heights. A volumetric problem was experienced when 5 ml was added as total volume. Since the absorption into the sponge was slow, about 2 ml of methanol was not retained in the sponge and overflowed from the wells. So, another group of sponges was cast with 5ml of silk solution and with different bed heights, but this time 3 ml and less methanol was added (D, E, F) to resolve this problem.

Table 3: In order to optimize the silk production process, 30 different samples were cast with different bed heights, methanol incubation time, salt solution and methanol amounts. The sample label was further used for identification during the characterization.

Samples	Bed height (cm)	Silk solution (ml)	Methanol amount (ml)	Incubation time (min)
A	1	5	5+3	30
B	1.2	5	5+3	30
C	1.4	5	5+3	30
D	1	5	3×2	30
E	1	4.5	3+2	30
F	1	4	3+1	30
G	1	5	3+2	30
H	1.2	5	2+1	30
I	1.4	5	2+1	30
J	1	5	2+1	30
K	1	4.5	1+0.5	30
L	1	4	1+0.5	30
M	1	4	3	60
N	1	4	3+2	60
O	1	4	3+1	60
P	1	4	3	60
R	1	4	3×2	60
S	1	4	3×3	60
T	1	4	3	30
U	1	4	3×2	30
V	1	4	3×3	30
W	1	4	3	60
X	1	4	3×2	60
Y	1	4	3×3	60
AA	1.2	5	3×2	30
AB	1.2	4.5	3×2	30
AC	1.2	4	3×2	30
AD	1.4	5	3×2	30
AE	1.4	4.5	3×2	30
AF	1.4	4	3×2	30

After determining the best amount that can be applied at one time, studies were started for the exposure time. In this context, applications were made 1, 2 and 3 times. In total, 8 different methanol amounts were tested. It was also concluded that different amounts of methanol had no visible effect on the sponges. All the cast sponges were analyzed by IR spectroscopy since in order to prove that methanol did not cause structural changes.

In order to observe the amount of methanol and incubation time, 2 groups of sponges containing 1 cm bed height and 4 ml silk solution were cast. The first group was incubated for 30 min with the following amounts 3, 3×2, 3×3 ml (T, U, V). The second group was incubated for 60 min with the same amounts as the first group: 3, 3×2, 3×3 ml (W, X, Y).

These sponges were then subjected to the specified characterization methods to determine the optimal sponge to conduct long-term stability and usability tests to validate the performance of the sponges in real-world applications.

3.2. Morphology of the Silk Sponges

The 30 sponges with different properties were cast into petri dish wells with a 3.5 cm diameter and first, examined using a range of visual standards.

One noteworthy finding was the obvious variation in the sponges' surface properties after the porogen was removed in dependency of porogen to silk solution ratio. Surface dispersion occurred in cases where the porogen to silk solution ratio was not as ideal as it should have been during the porogen removal stage. As a result of the visual evaluation, the bed height of 1.4 cm for all silk solution quantities used did not ensure high quality sponge production. Additionally, it was evident that higher ratios of bed height necessitated extended durations of hot water treatment to successfully eliminate porogens. This discovery highlights the intricate relationships that exist between the production parameters and the subsequent processing phases, particularly in relation to the surface morphology and porosity.

Another aspect of visual testing based on morphological properties pertained to the formation of a rigid external layer on the upper surface of the sponges. The diversity of this phenomena was seen in connection to the ratio of silk solution to porogen utilized in the fabrication procedure. Interestingly, differences in the hard top layer thickness were linked with changes in the silk solution/porogen ratio. There was a significant increase in hard top coat formation especially in sponges with a sponge thickness bed height of 1 cm. This layer's thicker forms were found to be undesirable since they could obstruct later experimental procedures, especially when it comes to in vitro testing. Developing a process for removing the hard top layer from the sponges became essential in order to lessen their impact on assessment methods. This technique made sure that the hard top layer would not get in the way of later analyses, allowing for a more accurate and trustworthy assessment of the silk sponge's properties. For these reasons, a bed height ratio of 1 cm was also not found to be effective. This occurrence emphasizes how important it is to maintain the proper ratio of silk solution to porogen, as deviations from it resulted in reduced surface integrity.

The investigation into the production of silk sponges uncovered a notable problem concerning the amount of methanol utilized, as determined through visual examination. An overflow occurred from the 3.5 cm diameter wells when attempting to use 5 ml, necessitating further examination of the maximum allowable quantity. The optimal methanol quantity should not exceed 3 ml, addressing challenges of potential inconsistencies like application challenges.

Another morphological assessment is the data obtained by SEM including enzymatic degradation effect on silk morphology. Using this method, the effect of salt bed height, methanol amount and incubation time as well as silk solution amount was investigated. Evaluation of SEM images from 30 samples

showed that there were few obvious morphological differences based on the comparison of sponges with different parameters at the microscopic level (see *Figure 6*). Comb-like structure was observed in all samples.

Furthermore, the sponge sample that underwent media washing was examined using the SEM (refer to Figure 6A). An observation was conducted to ascertain whether there are any discernible structural disparities between the standard sponge and the debris formations. It is thought that it is the FBS in the media content that causes this difference.

The preparation of samples is a crucial aspect that significantly impacts the results of SEM. In particular, samples should be cut into small pieces in such a way as to minimize damage to the integrity of the structure. The comb-like structure was not precisely observed in some samples due to image glitches, as demonstrated by multiple examples based on the pressure that had been applied during cutting. At the same time, this can be problematic during the gold-coating process since the surface is not well-cut. The reason for coating with gold is to add a conductive layer. This allows imaging at greater accelerating voltages and vacuum levels without any charge, so producing the best quality image. In poorly coated specimens, the images show glare and glitter bands in places. Naturally, this leads to a lack of good images.

Another interesting finding was detected during SEM. Visual examination verified these findings, showing that the sponge's top layer had substantially different integrity than the other sections (see Figure 6G). Under a microscope, this difference in structural integrity was even more noticeable than visual testing. The so-called middle part clearly shows a well-like structure, while the hard-top part shows a stiff structure. These finding highlights the need to remove the sponges' hard top coat prior to starting studies in order to guarantee consistency and dependability in the outcomes.

Moreover, images of silk sponges that had been digested by enzymes showed obvious symptoms of deterioration. Particular degradation pits that were ascribed to enzymatic activity were clearly visible with the protease and α-chymotrypsin enzymes (see Figure 6H and 6I). The gaps in the structure were even more pronounced in the protease enzyme then α-chymotrypsin. However, the greatest degradation was seen in the sponge exposed to both.

After comparing these pits to images of silk sponges that had not been digested, it became clear that the enzymes had a significant impact on the structure of the sponge. The purpose of this comparison is to illustrate how effectively enzymatic digestion can alter the morphology of sponges. This comparison offers valuable information for applications that require precise control over the degradation of sponge characteristics.

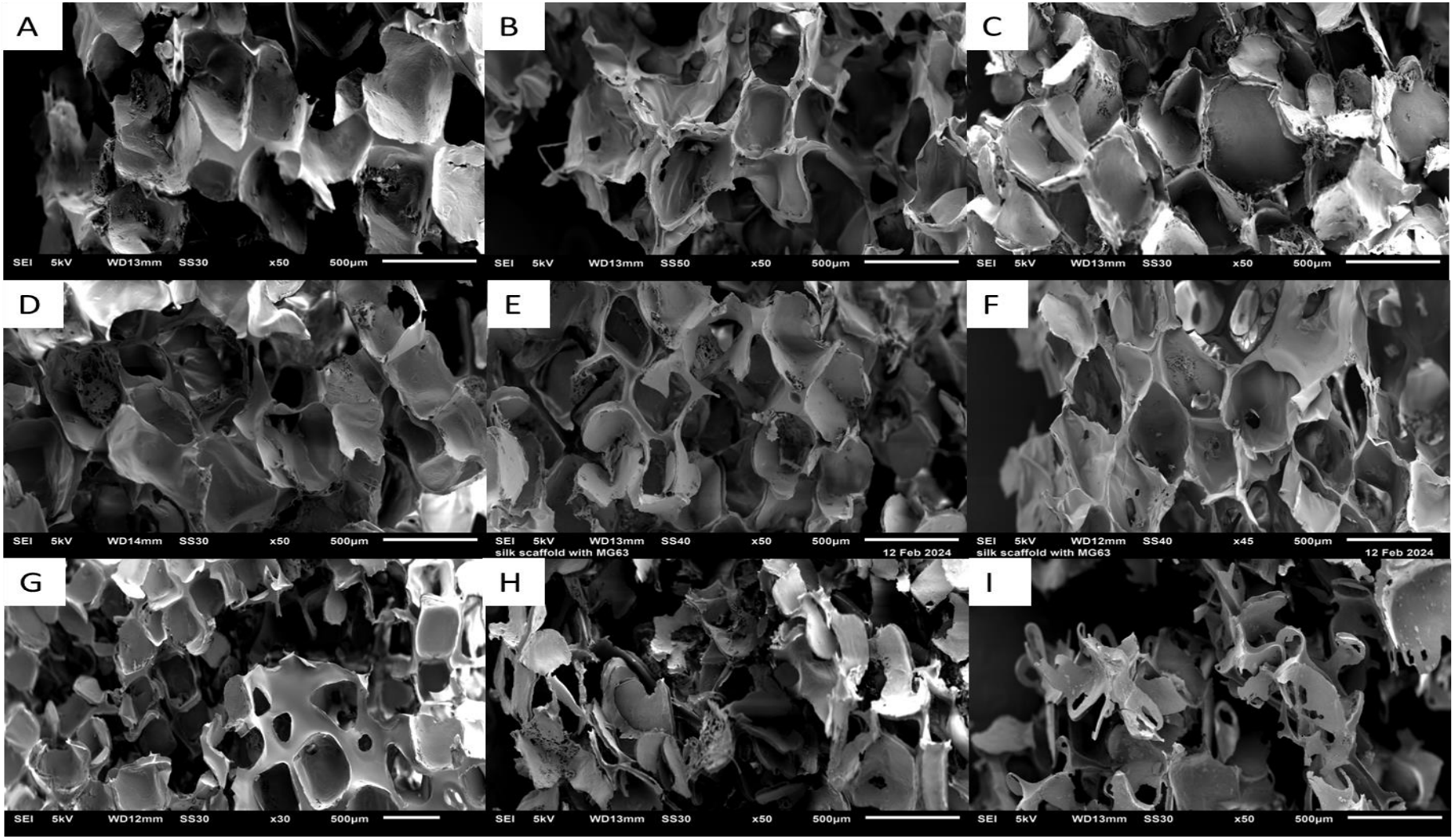

Figure 6: SEM images from the samples of silk sponges with different properties are shown. A) Sponge with washed in media B) Sponge with 1.2 cm bed height to 5ml silk solution 3+3 ml methanol, 30 Minutes Incubation C) Sponge with washed in media D) Sponge with 1 cm bed height to 4 ml silk solution 3+1 ml methanol exposure E) Sponge with 1 cm bed height to 4 ml silk solution, and 3 times 3 ml methanol exposure F) Sponge with 1 cm bed height to 5 ml silk solution G) Sponge with 1.4 cm salt bed height and 5 ml silk solution H) Protease applied silk sponge I) α-Chymotrypsin applied silk sponge

Considering these findings, it was decided that the sponge with 4.5 ml silk solution and 1.2 cm bed height was the best sponge for morphological properties. The methanol amount was defined as 3 ml with two times of exposure (see *Table 3A*). The amounts used for this sponge were calculated for a petri dish of 8.5 cm diameter to be able to produce bigger sponge (see *Table 3B*).

Table 4: Parameter details of optimized sponge is shown. A) Optimized sponge based on the morphological assessment B) Calculation for 8.5 cm diameter petri-dish.

A)

Property	Silk sponge Ø35 mm
Salt bed height	1.2 cm
Salt amount	16.8 g
Silk solution volume	4.5 ml
MeOH volume	3 ml
MeOH exposure	2×

B)

Property	Silk sponge Ø85 mm
Salt bed height	1.2 cm
Salt amount	100 g
Silk solution volume	25.5 ml
MeOH volume	17 ml
MeOH exposure	2×

3.3. Structural Assessment

Silk proteins are known to undergo a conformational transition from random coil or helical structures to β-sheet configurations when exposed to aqueous alcohol or salt solutions. This transition is essential for the development of stable silk sponges, and FTIR spectroscopy detects the ß- sheet configuration peaks. In total, all 30 silk sponges with different properties were examined in order to identify the structural changes.

This assay's primary objective is to systematically evaluate how methanol volume and incubation time influence silk sponge β-sheet structural induction and stabilization. This study evaluated the influence of incubation period (30 min and 60 min) on the formation of the β-sheet structure in SF sponges. According to the initial visual assessments, a quantity of 3 ml of methanol was utilized for each incubation time. Specifically investigated throughout the 30-min incubation period were three separate methanol amount application: a single application of 3 ml, two consecutive applications of 3 ml each, and three consecutive applications of 3 ml each. The SF sponges received the same methanol application methods throughout the one-hour incubation period. The conformational transition of silk proteins to β-sheet structures was to be found by means of a methodical technique, considering methanol amount and exposure period.

β-sheet structures are found by FTIR spectroscopy examination of SF sponges under several preparation circumstances. Two particular areas contain the characteristic β-sheet peaks: the amide I region, which corresponds to CO stretching vibrations and runs from 1600 to 1700 cm^{-1}; and the amide II region, which corresponds to secondary NH bending vibrations and ranges from 1500 to 1600 cm^{-1}. These special peaks confirm the development of β-sheet structures, which are necessary for preserving the structural integrity and functionality of the silk sponges. Usually connected with globular proteins, the amide III band correlates to the stretching of the C–N bond and ranges between 1350 to 1200 cm^{-1}. (156)

These two regions were analyzed for the sample of the 60- and 30-min incubation time. All samples showed consistent amide II peaks at 1515 cm^{-1} and amide I peaks at 1621 cm^{-1}, which are indicative of silk II structures, according to FTIR spectroscopic research (see *Figure 7*). A further observation of amide III peaks was made at 1232 cm^{-1} for all samples.

These results indicate that, independent of the methanol volume and methanol incubation duration, there were no variations in the β-sheet composition of the silk fibroin sponges. Under these experimental conditions, the conformational transition to β-sheet structures was not affected by differences in methanol amount and methanol incubation time, as seen by the stability of the β-sheet peaks.

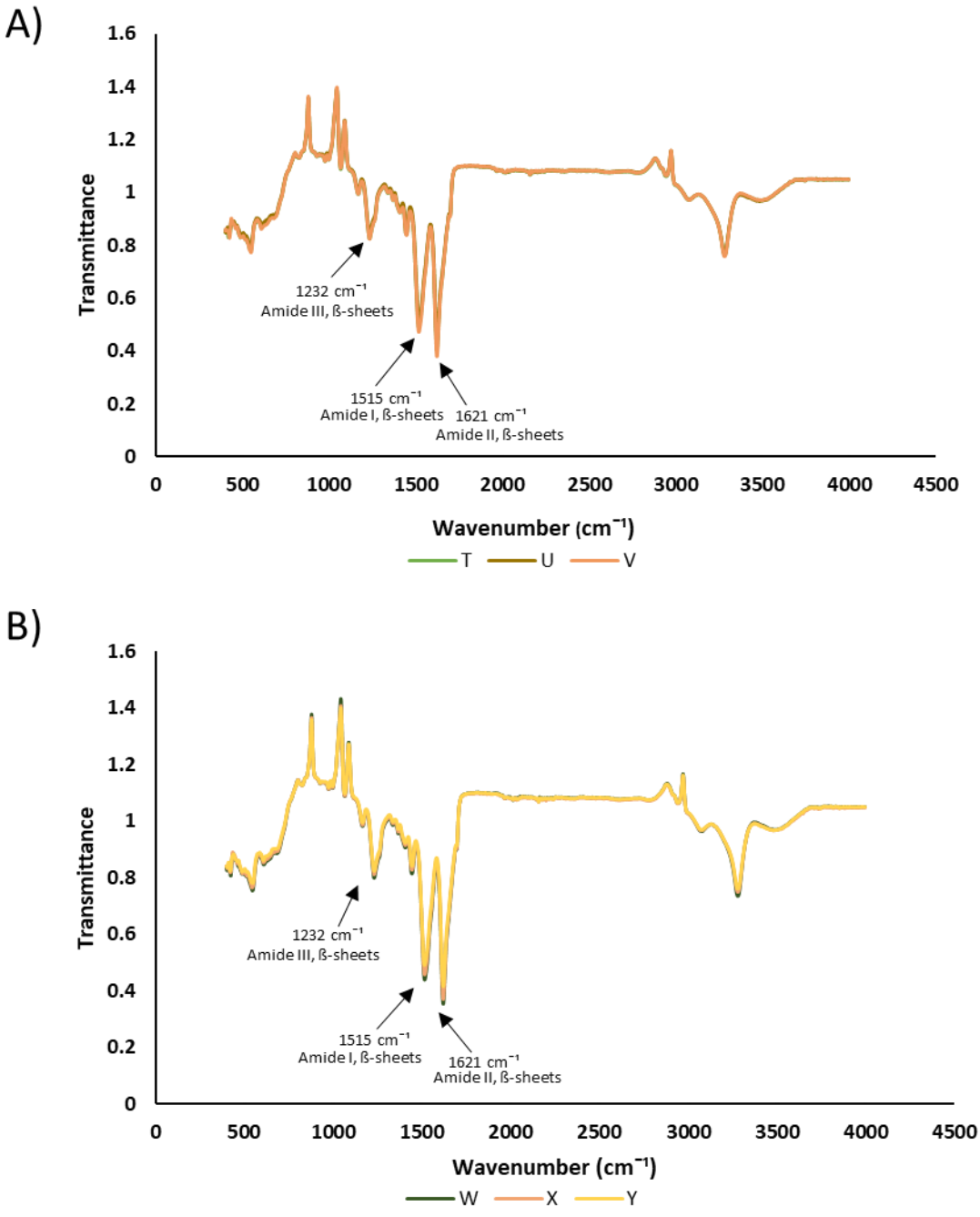

Figure 7: IR Spectra results from compared silk sponges. A) Three samples with different amounts of methanol were subjected to a 30 min incubation period and analyzed by IR spectroscopy to observe the effect of methanol. T: 3 ml methanol × 1, U: 3 ml methanol × 2, V: 3 ml methanol × 3 B) Three samples containing varying quantities of methanol were exposed to a 60-min incubation period and subsequently examined using IR spectroscopy to investigate the impact of methanol. W: 3 ml methanol × 1, X: 3 ml methanol × 2, Y: 3 ml methanol × 3.

To assess the influence of salt bed height on the β-sheet composition in silk fibroin sponges, we simultaneously analyzed and graphed the infrared data (see *Figure 8*). Three sponges were utilized, each containing identical quantities of methanol and silk solution. Each sponge was treated with two doses of 3 ml of methanol, with each dose containing 5 ml of silk solution. In order to determine the effect of bed height on the structural properties of silk sponges, the sponges were created at three different salt bed heights: 1 cm, 1.2 cm, and 1.4 cm.

The peaks were observed exactly at the same wavenumbers as methanol amount and incubation time comparison data. All samples showed consistent amide II peaks at 1515 cm^{-1} and amide I peaks at 1621 cm^{-1}, which are indicative of silk II structures. A further observation of amide III peaks was made at 1232 cm^{-1}. It was once again demonstrated that bed height (absolute amount) does not change the ß-sheet structure.

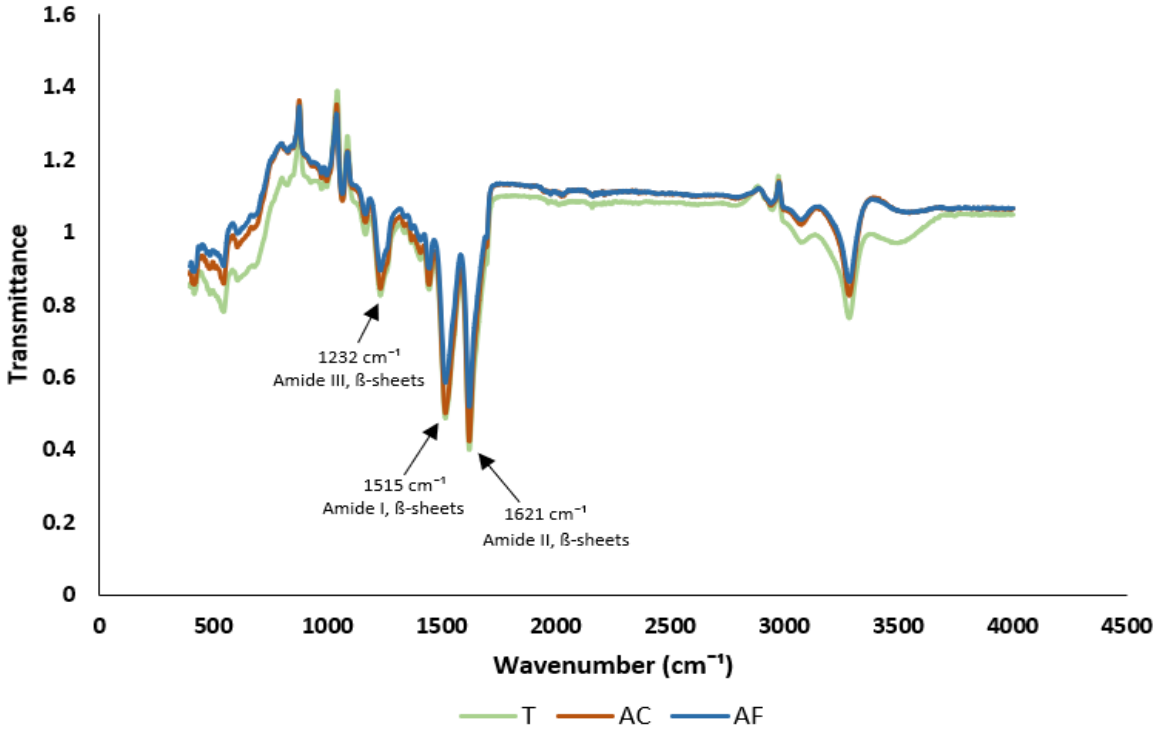

Figure 8: Three samples with 4 ml silk solution but different salt bed heights are subjected to IR spectroscopy for examine the effect of bed height in structural level. T: 1 cm, AC: 1.2 cm, AF: 1.4 cm

The conclusion that can be drawn from this is that when all of the samples are taken into consideration, there is no change in the ß-sheet peaks. The results of this experiment also indicated that the IR spectroscopy was not affected in any way by the height of the salt bed, the amount of silk solution, the amount of methanol, or the length of time that was spent incubating the methanol.

3.4. Water Volume and Swelling of Silk Sponges

All 30 samples with were analyzed to study the interaction of silk sponges with water. The accompanying table provides an overview of the average values from three repetitions of the evaluation of the water behavior of the samples (see *Table 5*).

It was decided to select sponges that had the different bed heights and same silk solution amount for the purpose of conducting comparative analysis. Two different sample groups were investigated and studied for the purpose of this evaluation.

Table 5: Average water retention (%), swelling ratio and water uptake (%) values for 30 samples from 3 repetitions. Details of the examples corresponding to the letters are in Table 3

Samples	Water Retention (%)	Swelling Ratio	Water Uptake (%)
A	3.6±0.6	11.3±2.4	91.7±1.5
B	3.7±1.4	10.1±4.3	90.2±3.1
C	3.5±0.4	13.2±2.3	92.8±1.2
D	4.0±0.9	11.6±2.8	91.8±1.9
E	5.1±0.8	12.6±2.5	92.5±1.3
F	4.1±1	9.9±2.1	90.6±2.1
G	4.6±0.7	9.5±0.7	90.4±0.7
H	4.8±1.1	10.3±3.6	90.4±3.7
I	4.0±0.6	10.8±2.8	91.1±2.4
J	4.6±0.9	10.6±1	91.4±0.7
K	4.6±0.9	10.7±2.4	91.2±1.7
L	3.6±0.5	9.4±1.7	90.2±1.5
M	6.5±3.1	10.3±2.2	90.9±1.9
N	3.9±0.8	12.4±2.9	92.3±1.9
O	3.6±0.6	9.8±1.7	90.6±1.6
P	4.1±1.8	11±3.1	91.3±2
R	3.3±0.3	9.6±3.5	89.7±3.8
S	3.6±0.3	11.3±0.8	91.9±0.5
T	6.1±3.6	11.5±3.7	91.5±2.4
U	3.5±0.9	10.3±1.5	91.0±1.3
V	3.4±0.5	9.9±2.3	90.5±1.9
W	3.3±0.7	8.8±0.7	89.8±0.7
X	3.0±0.6	9.5±1.6	90.3±1.4
Y	3.8±0.9	10.7±2.5	91.3±1.7
AA	3.2±0.6	9.5±0.7	90.5±0.6
AB	3.4±0.8	9.0±0.4	90.0±0.4
AC	3.7±0.6	9.7±2.6	90.3±2.4
AD	4.7±1.1	13.2±2.6	92.8±1.4
AE	4.0±1.1	11.7±0.2	92.2±0.1
AF	4.5±0.8	10.6±2.2	91.2±1.5

First group was the sponges prepared with 5 ml of silk solution and treated with 3 ml of methanol applied twice, casted at bed heights of 1 cm, 1.2 cm, and 1.4 cm (see *Figure 9*). The results indicate that bed height affects the way silk sponges absorb water, with certain heights leading to better swelling and water retention based on the comparison between the sponges that are having 1.2 cm to 1.4 cm bed height. Even tough, the sponge with a bed height of 1 cm does not meet this expectation, the standard deviation was quite small, this difference was not found to be significant.

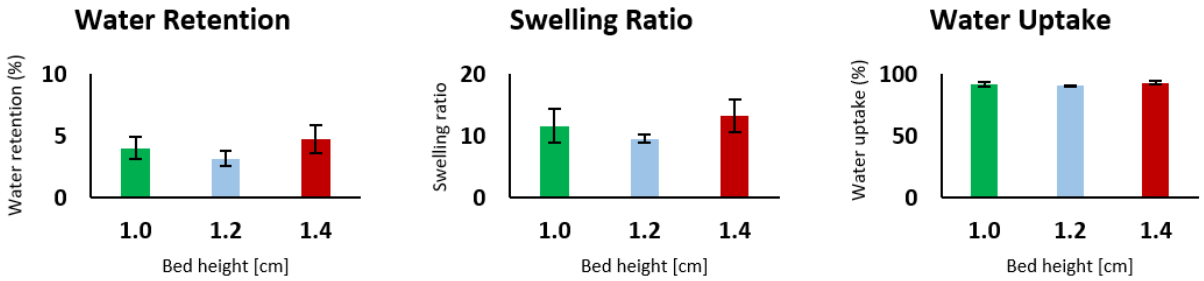

Figure 9: The water properties of the salt bed height parameter of the sponge samples were investigated. As first sample group, 3 samples with different bed heights were determined. Silk solution amount (5ml), methanol amount (3×2 ml) and incubation times (30 min) were kept constant for all samples.

The second sample set was then examined: a bed height of 1, 1.2 and 1.4 cm with 4 ml of silk solution, respectively (see *Figure 10).* These sponges exposed to 2 x 3 ml methanol and incubated for 30 min. This sample set revealed that the swelling ratio of the sponges and water retention were highly connected with bed height. When the bed height increased, water retention, swelling and water uptake also increased.

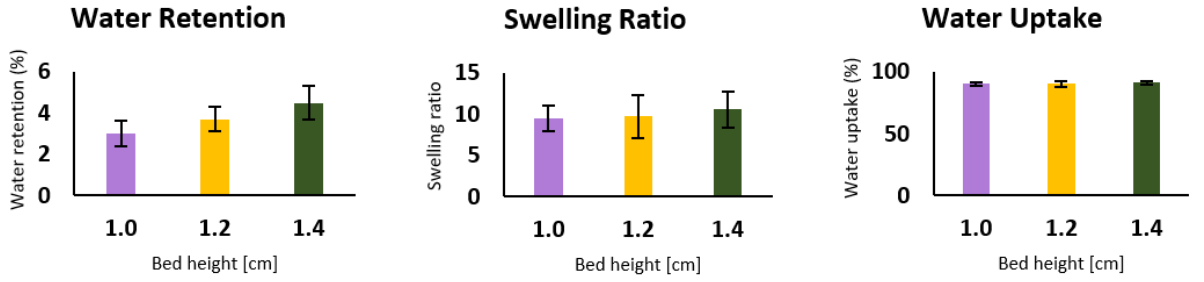

Figure 10: The second sample group was selected to examine the effect of salt bed height on water properties. This group is also consisting of 3 sponge samples with different bed heights. Silk solution amount (4 ml), methanol amount (3×2 ml) and incubation times (30 min) were kept constant for all samples as in the first sample group.

Based on these sample evaluations, the results reveal that, generally, bed height significantly affects the capacity of silk sponges to water retention, swelling ratio and water uptake.

Furthermore, another examination was performed to find out the water behavior relation of sponges with varying silk solution volumes but the same bed height, methanol amount, and incubation time. This study was based on two distinct groups. The first set of sponges had a bed height of 1.2 cm and 3 ml of methanol were applied twice with 30 min of incubation time. Silk solution was applied in three volumes: 4, 4.5, and 5 ml (see *Figure 11*).

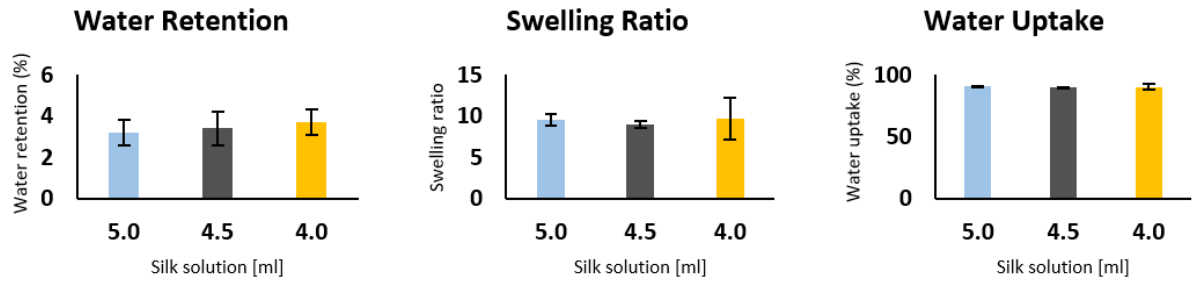

Figure 11: The water properties of the silk solution's amount in the sponge samples were examined. Salt bed height (as 1.2 cm), methanol amount (3×2 ml) and incubation times (30 min) were kept constant for all samples.

The tendency that was identified by the experiment was that lower volumes of silk solution were correlated with stable water absorption values. On the other hand, sponges having smaller volumes of silk solution also showed similar water retention percentages in the water retention data, which showed an inverse link. Interestingly, the sponge that had the smallest volume of silk solution also had the highest percentage of water retention. It also be noted that, the sponge containing 4 ml of silk solution had a larger standard deviation than the other sponges, according to the swelling ratio data analysis. As such, it was difficult to definitively demonstrate a swelling association between the sponges. These results point to complex relationships between the volume of the silk solution and the properties of the water behavior in the artificial sponges that are rather similar.

The fourth batch of sponges received two 3 ml methanol injections and had a bed height of 1.4 cm. The amounts of the silk solutions also changed; from 5 ml to 4.5 ml to 4 ml (see *Figure 12*). The diminishing trend in the swelling and water absorption ratios was linked to the amount of the silk solution declining

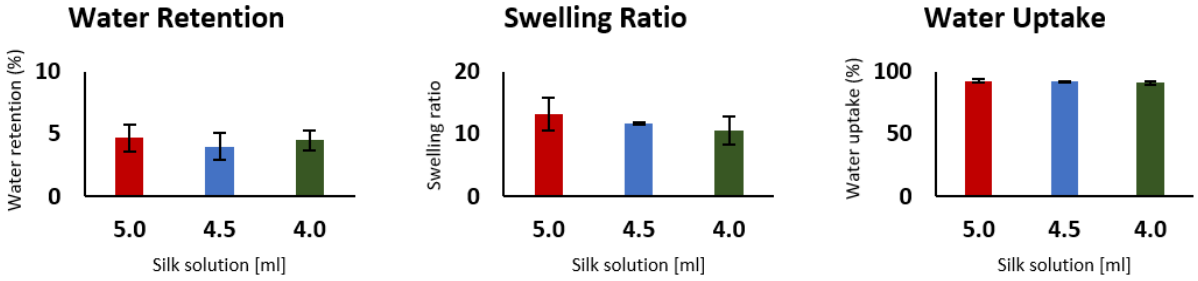

Figure 12: The fourth sample group was selected to examine the effect of silk solution amount on water properties. In here, salt bed height (as 1.2 cm), methanol amount (3×2 ml) and incubation times (30 min) were kept constant for all samples as in the first sample group.

These two independent test groups were established as further evaluation to observe how much methanol changed the behavior of the water under controlled silk solution volume and bed height circumstances.

For the fifth test group, sponge preparation consisted in a 1 cm bed height and 4 ml of silk solution (see *Figure 13).* The amount of methanol was gradually increased in each sponge, going from one application of 3 ml to three applications in a row. The sponges were then incubated for 30 minutes in order to promote the conformational shift of the silk proteins.

The result graphs for this group were evaluated, it was discovered that the amount of methanol used resulted in same values in water retention, swelling ratio, and water uptake values. The fact that this is the case shows that the quantity of methanol that is present in the silk sponges do not interfere with water behavior parameters.

On the other hand, it is essential to take into consideration the fact that the sample that has been subjected to methanol in the past exhibited a relatively high standard deviation. Whether or if the 30 min methanol incubation period is to blame for this unexpected fluctuation is nothing that has been determined at this time. It is required to do additional research in order to determine the core rationale about this aberration.

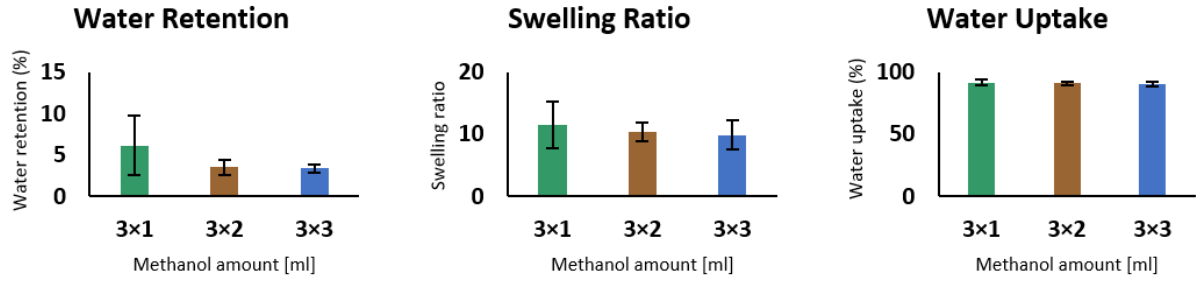

Figure 13: As another evaluation, the effect of the amount of methanol was examined. In this context, 3 sample sponges were selected for the first research group. Silk solution amount (4 ml), bed height (1 cm), and incubation time (30 min) are constant for all samples.

Casting the sixth test group, which comprised of sponges with a bed height of 1 cm and was exposed to 4 ml of silk solution, was accomplished in a manner that was analogous to the casting process used for the fifth test group (see *Figure 14*). The duration of the methanol exposure varied within this group. In particular, the sponges were exposed to two different exposure durations to 3 ml of methanol. The sponges were then incubated for 1 h in order to promote the structural change of the silk proteins.

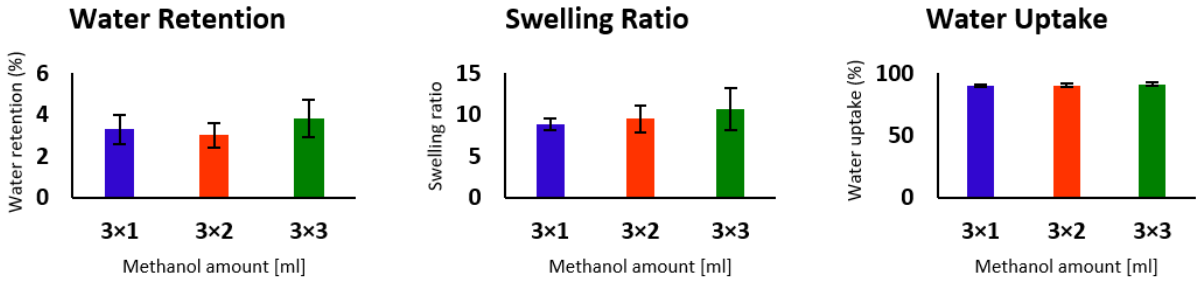

Figure 14: The sixth examination group based on methanol amount effect on water behavior consisted of 3 samples as well. Silk solution amount (4 ml), bed height (1 cm), and incubation time (1 h) are constant for all samples.

The collected data indicates that there is no significant effect of methanol on sponges and water intake and swelling ratio values showed similar values for the sixth test group.

3.5. Cell Viability

In this study, the MTT assay was utilized to explore the potential cytotoxic effects of HFIP and methanol, which are utilized in the production of silk sponges, as well as the impact of salts in cell culture media on the survival of cells. Through the application of a methodical strategy, the viability of the cells was evaluated in a variety of concentrations of these plates.

The results first have been analyzed for 3 plates individually including blank data. After subtracting the average value of DMSO, comparison to blank values had been calculated. Afterwards, the average values of three repetitions were compared to the values from blank row for each plate. There was no significant difference in the results from the 0 h to the 114 h. However, the 168 h demonstrated a significant outcome as "*" (see *Figure 15).* So, hereby significance value for 168th hour is less than or equal to 0.05.

This result demonstrated that the toxic effects of HFIP and methanol become significant enough to harm cells after an exposure period of 168 h. This indicates that prolonged exposure to these chemicals can be detrimental to cellular health, emphasizing the importance of monitoring and regulating their use to prevent potential cellular damage. The findings highlight the necessity for caution in environments where these substances are present, particularly over extended timeframes.

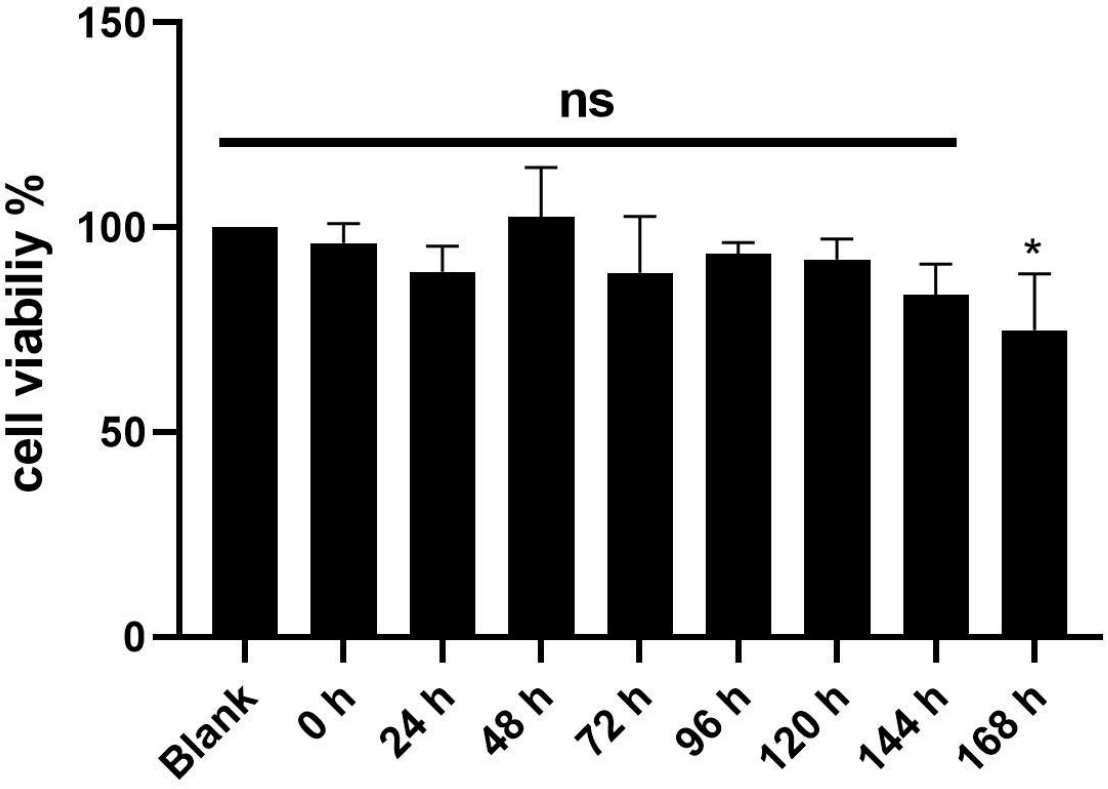

*Figure 15: Significance calculations were performed to detect the level of toxicity. The calculation was made based on the comparison to blank value. The values from 0 h to 114 h showed no significance. However, 168 h was showed a significance. The significance is defined as * p ≤ 0.05, ** p ≤ 0.01, *** p ≤ 0.001 **** p ≤ 0.0001. ns: non-significant. Created by GraphPad Prism.*

3.6. Irradiation Studies

In this study, the stability of sponges created from regenerated silk were assessed when exposed to gamma irradiation compared to enzymatic digested samples. Two different ways were used to evaluate the possibility of radiation sterilization in the creation of silk scaffolds in large quantities.

3.6.1. CD Measurements

The samples were subjected to the irradiation process with dosages of 0, 2, 5, 10, 25, 50, 100, 250, 500 Gy. The sterilization process involved exposing the samples to an absorbed dose of 25 kGy (see *Figure 16A*). The investigation was conducted using irradiation dosages spanning a wide range from 2 - 25 kGy since the effect of irradiation against silk fibroin sponges is not well known.

Positive controls were samples undergoing protease XIV and α-chymotrypsin digestion against which the findings were evaluated (see *Figure 16B*). Using CD spectrophotometric analysis, the secondary structures of both irradiated and digested silk samples were investigated. Based on the negative peak in the CD spectra of the irradiated materials at 200 and 205 nm, the existence of ordered structures is linked with the negative Cotton effect. This negative peak in the broken-down samples moved to 205–

210 nm. At roughly 197 nm no maximum signal was observed, suggesting the presence of the silk I structure. The studied irradiation dosages had no effect on the stability of silk fibroin since no evident effects were identified.

At roughly 205–210 nm, the CD spectra of the digested silk samples revealed a negative Cotton effect—that is, a clear change in absorption down to negative values. Moreover, the digested silk samples possessed an ellipticity one unit higher in millidegrees than the irradiated samples.

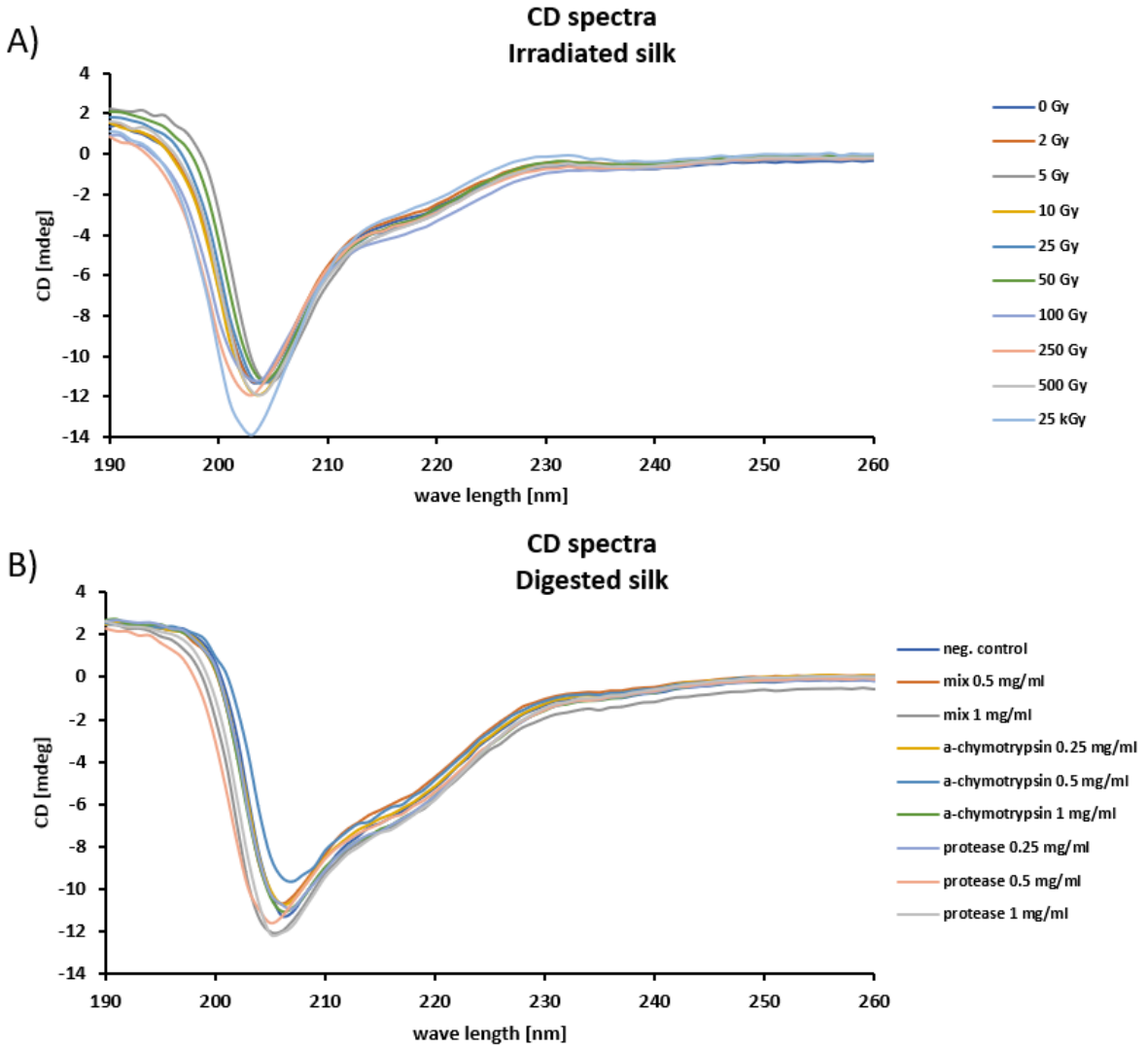

Figure 16: The CD measurement results were investigated under two graphs. A) The samples were subjected to escalating radiation doses, ranging from 0 to 500 Gy, including intermediate doses of 2, 5, 10, 25, 50, 100, and 250 Gy. Additionally, a sample was sterilized using a dosage of 25 kGy. CD Spectroscopy was performed to examine all the irradiated samples. The CD spectra of the irradiated silk exhibited a negative cotton effect, indicating the presence of ordered structures. Additionally, a peak at around 200 nm was observed, which corresponds to the random coiled conformation. The irradiation samples exhibit a decrease in intensity at wavelengths ranging from 205 to 210 nm, known as the negative shoulder. B) The positive control for the experiment consisted of samples that were treated with two enzymes, Protease XIV and α-chymotrypsin. The samples were digested using these enzymes. The control samples included a blank (B), α-chymotrypsin at concentrations of 0.25, 0.5, and 1 mg/ml (α-Chym), protease XIV at concentrations of 0.25, 0.5, and 1 mg/ml (Prot), and a mixture of protease and α-chymotrypsin in a 1:1 ratio at concentrations of 0.5 and 1 mg/ml (Mix). The CD spectra of the digested silk exhibited a negative cotton effect, indicating the presence of organized structures. Additionally, a peak at around 200 nm was observed, which corresponds to the random coiled conformation. The negative shoulder is observed in the irradiated samples at wavelengths ranging from 205 to 210 nm, and in the digested samples at wavelengths ranging from 200 to 205 nm.

3.5.2. SDS PAGE & Western Blot

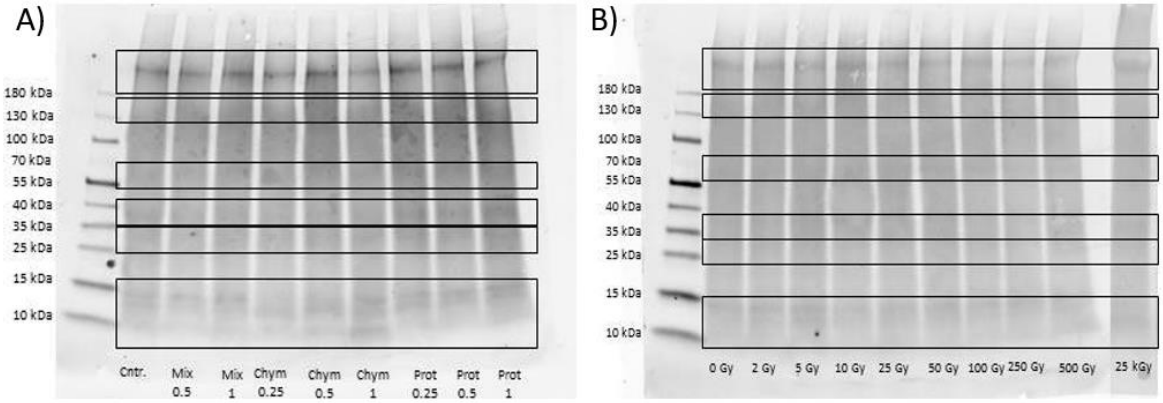

Figure 17: SDS-PAGE was performed for molecular weight analysis. A) enzymatic digestion samples B) irradiated samples. The left column has a pre-stained ladder that was divided during the same run to demonstrate various protein weights.

In order to ascertain whether the digestion and radiation caused any possible degradation of the silk sponge, a molecular weight analysis of protein fragments utilizing an SDS-PAGE and Western Blot was carried out (see *Figure 17*). The sponge samples were dissolved in 9M LiBr. The scaffolds dissolved in LiBr solution showed very little degradation, indicating that the silk sponge was stable in these at these conditions. (157)

The findings displayed for the SDS-PAGE indicated the polydisperse population, as indicated by the literature. (158) Bands that exhibit varying degrees of protein fragmentation and have molecular weights of roughly 15, 25, 37, 60, 130, and 200 kDa are indicative of the silk characteristics of these bands. It is interesting to note that the 25 kDa band corresponds to the light chain of silk fibroin. According to Wang et al., the existence of a band with a molecular weight of 200 kDa indicates that the silk fibroin has undergone mild degradation. (159)

The silk samples digested by α-chymotrypsin showed distinct bands, especially those containing degraded protein fragments with a molecular weight of about 10 kDa. Also, more defined bands were seen at degraded samples Furthermore, a band that was more intense and had a molecular weight greater than 180 kDa was seen, suggesting distinct protein component aggregation or breakdown. The appearance of bands in the positive controls that are roughly 10 kDa indicates that the silk fibroin protein chains have severely degraded.

4. Conclusion

This thesis has successfully improved silk sponge production. A major challenge in biomedical research is being tackled through the creation of a standardized manufacturing process for scaffolds, ensuring that they can be produced on a large scale and replicated consistently. Comprehensive data was collected from 30 different samples, which were evaluated from many different perspectives.

The visual testing findings demonstrate how important it is to carefully control fabrication parameters to ensure silk sponge creation is consistent and of a high caliber. The results highlight the intricate nature of producing silk sponges and the importance of optimizing fabrication conditions to achieve the desired morphological features. This study improves the techniques used to create silk sponges, enhancing their suitability for biological purposes, by elucidating the relationship between the formation of the outer layer and the ratio of silk solution to porogen.

The silk sponges' intricate morphology was revealed by SEM, which also revealed no microscopic variations in terms of overall integrity. On the other hand, clear distinctions between the intermediate

section and the hard top layer of the sponge were revealed through visual comparisons between digested silk and normal morphology. This morphological difference draws attention to the sponges' internal structural integrity. These results highlight how crucial it is to comprehend the internal structure of silk sponges in order to maximize their performance and design for certain applications.

The FTIR study revealed that the creation of silk fibroin scaffolds triggers a conformational transition from a random coil structure to a ß-sheet structure. It is noteworthy that the transition did not show any noticeable variation based on the amount of methanol or the period of incubation. This suggests that these factors did not influence the formation of the ß-sheet structure.

How successfully silk sponges absorb water and swell and hold it depends in great part on the volume of the silk solution, salt bed height, and methanol treatment. The height of salt bed substantially did not show any differences for silk sponges absorb and hold water based on the two sample sets. The methanol treatment differences on sponges were indicated a stable relationship with water retention, swelling ratio, and water uptake values. Understanding these relationships can help one to maximize the design and functionality of silk sponges for application in automated systems.

In addition, this work provided significant insights into the cytotoxic effects of the critical components used in cell culture and silk sponge manufacture. The study significantly enhances our comprehension of silk-based materials in biomedical applications by elucidating the safety and biocompatibility aspects involved. The results showed that the salts in the cell culture medium and the solvents methanol and HFIP had a significant cytotoxic effect. The HT-29 cells are adversely affected by these chemicals, as evidenced by the observed decrease in cell viability over time.

While the amount of methanol and length of incubation do not significantly affect the structural integrity of silk fibroin scaffolds, careful consideration must be given to the cytotoxic characteristics of certain solvents and salts. The results presented above emphasize how important it is to improve the chemical environment in order to ensure the safety and effectiveness of scaffolds made from silk in biological settings.

Based on the results of CD spectroscopy, it was determined that the irradiation dosages that were investigated did not have any impact on the stability of silk fibroin. By revealing distinct protein fragments spread across a variety of molecular weight ranges, the SDS-PAGE analysis reveals that the silk sponge is susceptible to enzymatic digestion as well as radiation-induced disintegration. Gamma-irradiation has been shown to be an effective approach for sterilizing silk fibroin sponges, as demonstrated by both of the experiments. This opens the door for a wider range of biological applications of silk fibroin.

This research also showed another aspect. The structure of silk fibroin has been revealed to be severely damaged and degraded by Protease XIV and α-chymotrypsin, as demonstrated by the findings of the study by SDS-PAGE, CD measurement and SEM.

After conducting comprehensive evaluations of bed height, silk solution volume, and methanol treatment, it was determined that the optimal sponge structure for irradiation tests had a bed height of 1.2 cm and a silk solution volume of 4.5 ml 3×2 ml methanol with 30 min incubation time due to its superior performance in preliminary assessments. The selected arrangement was chosen because to its favorable equilibrium features, all of which are crucial for the intended experimental purposes. The need of modifying the structural properties of silk sponges to achieve the desired performance characteristics is highlighted by this decision. Future research should aim to further change these features in order to enhance the usefulness and appropriateness of silk sponges in various silk-based

therapeutic applications. It was also revealed that visual testing, SEM, FTIR, water behavior testing, CD spectroscopy, SDS-PAGE and MTT methods were very successful in characterization of silk sponges.

Further refinement of the bed height and silk solution ratios were explored to optimize porosity and mechanical strength. As well as, investigation of other potential additives or treatments that could enhance the sponge properties without compromising structural integrity was performed with several methods. Long-term stability and usability of silk sponges was successfully conducted to ensure the sponges' performance in practical applications.

Scaffold-based 3D cell cultures are valuable tools in the research of cancer since they provide a more accurate representation of tumor biology than conventional 2D cultures. Many scaffold materials and procedures are currently under investigation, and each has unique advantages. The ongoing development of these models will help researchers to better understanding of cancer and speed the discovery of effective treatments.

The development of a 3D scaffold-based approach for additional medication and treatment related studies marks a turning point in preclinical cancer research. By increasing the accuracy and predictive value of preclinical studies and providing a more physiologically suitable environment for cell development and interaction, this breakthrough method lowers the need for animal testing. Because of the scaffold-based methods are enhanced the capacity to reproduce in vivo conditions, it conforms with ethical standards and promotes the worldwide attempt to minimize the use of animals in scientific research.

Clearly, the advances shown in this thesis mark a significant development in the field of cancer research, therefore advancing ethical as well as science. This 3D scaffold approach provides a more accurate and ethical way to preclinical research, hence enabling improved therapy approaches and a better knowledge of cancer studies using human colon cancer cells.

List of Abbreviations

Abbreviations	Definitions
2D	Two-dimensional
3D	Three-dimensional
CD	Circular dichroism
DBM	Demineralized bone matrix
DMSO	Dimethyl sulfoxide
ECM	Extra-cellular matrix
FBS	Fetal bovine serum
GelMA	Gelatin methacryloyl
H	Heavy
HA	Hyaluronic acid
HEMA	hydroxyethyl methacrylate
HFIP	1,1,1,3,3,3-hexa-fluoro isopropanol
HDP	Hanging drop plates
HMSC	Human mesenchymal stem cells
IR	Infrared
L	Light
MTT	(3-(4,5-dimethylthiazol-2-yl)-2,5-diphenyltetrazolium bromide)
Na_2CO_3	Sodium carbonate
NaCl	Sodium chloride
PBS	Phosphate-buffered saline
RPMI	Roswell Park Memorial Institute
RSF	Regenerated silk fibroin
SDS-PAGE	Sodium dodecyl-sulfate polyacrylamide gel electrophoresis
SEM	Scanning electron microscopy

SF	Silk Fibroin
SL	Soft lithography
TE	Tissue Engineering
TM	Tympanic membrane
UVL	Ultraviolet lithography

List of Figures

List of Tables

References

1. Bucciarelli A, Motta A. Use of Bombyx mori silk fibroin in tissue engineering: From cocoons to medical devices, challenges, and future perspectives. Biomater Adv. 2022 Aug; 139:212982. doi: 10.1016/j.bioadv.2022.212982. Epub 2022 Jun 11. PMID: 35882138.
2. Roblin NV, DeBari MK, Shefter SL, Iizuka E, Abbott RD. Development of a More Environmentally Friendly Silk Fibroin Scaffold for Soft Tissue Applications. J Funct Biomater. 2023 Apr 18;14(4):230. doi: 10.3390/jfb14040230. PMID: 37103320; PMCID: PMC10143335
3. R.J. Herrera, R. Garcia-Bertrand, The silk roads, in: Ancestral DNA, Hum. Orig. Migr, Elsevier, 2018, pp. 511–557, https://doi.org/10.1016/B978-0-12-804124- 6.00014-8.
4. H. Xiang, X. Liu, M. Li, Y. Zhu, L. Wang, Y. Cui, L. Liu, G. Fang, H. Qian, A. Xu, W. Wang, S. Zhan, The evolutionary road from wild moth to domestic silkworm, Nat. Ecol. Evol. (2018), https://doi.org/10.1038/s41559-018-0593-4.
5. Vepari C, Kaplan DL. Silk as a Biomaterial. Prog Polym Sci. 2007;32(8-9):991-1007. doi: 10.1016/j.progpolymsci.2007.05.013. PMID: 19543442; PMCID: PMC2699289.
6. Kundu, S. C., Dash, B. C., Dash, R. & Kaplan, D. L. Natural protective glue protein, sericin bioengineered by silkworms: potential for biomedical and biotechnological applications. Prog. Polym. Sci. 33, 998–1012 (2008).
7. Q. Wang, S. Ling, Q. Yao, Q. Li, D. Hu, Q. Dai, D.A. Weitz, D.L. Kaplan, M. J. Buehler, Y. Zhang, Observations of 3 nm silk nanofibrils exfoliated from natural silkworm silk fibers, ACS Mater. Lett. 2 (2020) 153–160, https://doi.org/ 10.1021/acsmaterialslett.9b00461
8. Aramwit P, Siritientong T, Srichana T. Potential applications of silk sericin, a natural protein from textile industry by-products. Waste Manag Res. 2012 Mar;30(3):217-24. doi: 10.1177/0734242X11404733. Epub 2011 May 9. PMID: 21558082.
9. S.W. Ha, H.S. Gracz, A.E. Tonelli, S.M. Hudson, Structural study of irregular amino acid sequences in the heavy chain of Bombyx mori silk fibroin, Biomacromolecules (2005), https://doi.org/10.1021/bm050294m
10. L.-D. Koh, Y. Cheng, C.-P. Teng, Y.-W.K. Khin, X.-J. Loh, S.-Y. Tee, M. Low, E. Ye, H.-D. Yu, Y.-W. Zhang, M.-Y. Han, Structures, mechanical properties and applications of silk fibroin materials, Prog. Polym. Sci. 46 (2015) 86–110, https://doi.org/10.1016/j.progpolymsci.2015.02.001.
11. Z. Hao, D. Long, Y. Zhang, D. Umuhoza, J. Dai, Z. Xu, G. Zhang, W. Meng, Z. Xiang, A. Zhao, New insight into the mechanism of in vivo fibroin self-assembly and secretion in the silkworm, Bombyx mori, Int. J. Biol. Macromol. 169 (2021) 473–479, https://doi.org/10.1016/j.ijbiomac.2020.12.132.
12. M.S. Zafar, D.J. Belton, B. Hanby, D.L. Kaplan, C.C. Perry, Functional material features of Bombyx mori silk light versus heavy chain proteins, Biomacromolecules (2015), https://doi.org/10.1021/bm501667j.
13. T. Asakura, Structure of silk I (Bombyx mori silk fibroin before spinning) -type ii β-turn, not α-helix, Molecules 26 (2021) 3706, https://doi.org/10.3390/molecules26123706.
14. Y. Qi, H. Wang, K. Wei, Y. Yang, R.Y. Zheng, I.S. Kim, K.Q. Zhang, A review of structure construction of silk fibroin biomaterials from single structures to multilevel structures, Int. J. Mol. Sci. (2017), https://doi.org/10.3390/ijms18030237.
15. D. Wilson, R. Valluzzi, D. Kaplan, Conformational transitions model silk peptides, Biophys. J. (2000), https://doi.org/10.1016/S0006-3495(00)76813-5.
16. Reizabal A, Fidalgo-Marijuan A, Gonçalves R, Gutiérrez-Pardo A, Aguesse F, Pérez-Álvarez L, Vilas-Vilela JL, Costa CM, Lanceros-Mendez S. Silk fibroin and sericin polymer blends for sustainable battery separators. J Colloid Interface Sci. 2022 Apr; 611:366-376. doi: 10.1016/j.jcis.2021.12.067. Epub 2021 Dec 14. PMID: 34959010.

17. J.-H. Wu, Z. Wang, S.-Y. Xu, Preparation and characterization of sericin powder extracted from silk industry wastewater, Food Chem. 103 (4) (2007) 1255–1262.
18. Teuschl AH, van Griensven M, Redl H. Sericin removal from raw Bombyx mori silk scaffolds of high hierarchical order. Tissue Eng Part C Methods. 2014 May;20(5):431-9. doi: 10.1089/ten.TEC.2013.0278. Epub 2014 Feb 28. PMID: 24066942.
19. Nguyen TP, Nguyen QV, Nguyen VH, Le TH, Huynh VQN, Vo DN, Trinh QT, Kim SY, Le QV. Silk Fibroin-Based Biomaterials for Biomedical Applications: A Review. Polymers (Basel). 2019 Nov 24;11(12):1933. doi: 10.3390/polym11121933. PMID: 31771251; PMCID: PMC6960760.
20. Blamires, Sean & Spicer, Patrick & Flanagan, Patricia. (2020). Spider Silk Biomimetics Programs to Inform the Development of New Wearable Technologies. Frontiers in Materials. 7. doi: 10.3389/fmats.2020.00029.
21. Gosline JM, Guerette PA, Ortlepp CS, Savage KN. The mechanical design of spider silks: from fibroin sequence to mechanical function. J Exp Biol. 1999 Dec;202(Pt 23):3295-303. doi: 10.1242/jeb.202.23.3295. PMID: 10562512.
22. Sun W, Gregory DA, Tomeh MA, Zhao X. Silk Fibroin as a Functional Biomaterial for Tissue Engineering. Int J Mol Sci. 2021 Feb 2;22(3):1499. doi: 10.3390/ijms22031499. PMID: 33540895; PMCID: PMC7867316.
23. Zhang C, Zhang Y, Shao H, Hu X. Hybrid Silk Fibers Dry-Spun from Regenerated Silk Fibroin/Graphene Oxide Aqueous Solutions. ACS Appl Mater Interfaces. 2016 Feb 10;8(5):3349-58. doi: 10.1021/acsami.5b11245. Epub 2016 Jan 29. PMID: 26784289.
24. O'Brien F.J. Biomaterials & scaffolds for tissue engineering. Mater. Today. 2011;14:88–95.
25. Melke J., Midha S., Ghosh S., Ito K., Hofmann S. Silk fibroin as biomaterial for bone tissue engineering. Acta Biomater. 2016; 31:1–16. doi: 10.1016/j.actbio.2015.09.005.
26. Sakabe H., Ito H., Miyamoto T., Noishiki Y., Ha W.S. In vivo blood compatibility of regenerated silk fibroin. Sen'i Gakkaishi. 1989; 45:487–490. doi: 10.2115/fiber.45.11_487.
27. Santin M., Motta A., Freddi G., Cannas M. In vitro evaluation of the inflammatory potential of the silk fibroin. J. Biomed. Mater. Res. 1999; 46:382–389. doi: 10.1002/(SICI)1097-4636(19990905)46:3<382: AID-JBM11>3.0.CO;2-R.
28. Panilaitis B., Altman G.H., Chen J., Jin H.-J., Karageorgiou V., Kaplan D.L. Macrophage responses to silk. Biomaterials. 2003; 24:3079–3085. doi: 10.1016/S0142-9612(03)00158-3.
29. Meinel L., Hofmann S., Karageorgiou V., Kirker-Head C., McCool J., Gronowicz G., Zichner L., Langer R., Vunjak-Novakovic G., Kaplan D.L. The inflammatory responses to silk films in vitro and in vivo. Biomaterials. 2005;26:147–155. doi: 10.1016/j.biomaterials.2004.02.047.
30. Unger RE, Peters K, Wolf M, Motta A, Migliaresi C, Kirkpatrick CJ. Endothelialization of a non-woven silk fibroin net for use in tissue engineering: growth and gene regulation of human endothelial cells. Biomaterials. 2004 Sep;25(21):5137-46. doi: 10.1016/j.biomaterials.2003.12.040. PMID: 15109837.
31. Lawrence BD, Marchant JK, Pindrus MA, Omenetto FG, Kaplan DL. Silk film biomaterials for cornea tissue engineering. Biomaterials. 2009 Mar;30(7):1299-308. doi: 10.1016/j.biomaterials.2008.11.018. Epub 2008 Dec 6. PMID: 19059642; PMCID: PMC2670567.
32. Vollrath F, Knight DP. Liquid crystalline spinning of spider silk. Nature. 2001 Mar 29;410(6828):541-8. doi: 10.1038/35069000. PMID: 11279484.
33. Servoli E, Maniglio D, Motta A, Migliaresi C. Folding and assembly of fibroin driven by an AC electric field: effects on film properties. Macromol Biosci. 2008 Sep 9;8(9):827-35. doi: 10.1002/mabi.200800057. PMID: 18528847.
34. Kunhamed, Rahmathullavk. (2012). Management of Climatic Factors for Successful Silkworm (Bombyx mori L.) Crop and Higher Silk Production: A Review. Psyche. 2012. 10.1155/2012/121234.

35. Teulé F, Miao YG, Sohn BH, Kim YS, Hull JJ, Fraser MJ Jr, Lewis RV, Jarvis DL. Silkworms transformed with chimeric silkworm/spider silk genes spin composite silk fibers with improved mechanical properties. Proc Natl Acad Sci U S A. 2012 Jan 17;109(3):923-8. doi: 10.1073/pnas.1109420109. Epub 2012 Jan 3. PMID: 22215590; PMCID: PMC3271896.
36. Hu K, Cui F, Lv Q, Ma J, Feng Q, Xu L, Fan D. Preparation of fibroin/recombinant human-like collagen scaffold to promote fibroblasts compatibility. J Biomed Mater Res A. 2008 Feb;84(2):483-90. doi: 10.1002/jbm.a.31440. PMID: 17618493.
37. Wang Y, Kim UJ, Blasioli DJ, Kim HJ, Kaplan DL. In vitro cartilage tissue engineering with 3D porous aqueous-derived silk scaffolds and mesenchymal stem cells. Biomaterials. 2005 Dec;26(34):7082-94. doi: 10.1016/j.biomaterials.2005.05.022. PMID: 15985292.
38. Wang Y, Blasioli DJ, Kim HJ, Kim HS, Kaplan DL. Cartilage tissue engineering with silk scaffolds and human articular chondrocytes. Biomaterials. 2006 Sep;27(25):4434-42. doi: 10.1016/j.biomaterials.2006.03.050. Epub 2006 May 4. PMID: 16677707.
39. Ray LG. The Role of Synthetic Fibers in the Textile Industry of the Future. Textile Research Journal. 1952;22(2):144-151. doi:10.1177/004051755202200213
40. Altman GH, Diaz F, Jakuba C, Calabro T, Horan RL, Chen J, Lu H, Richmond J, Kaplan DL. Silk-based biomaterials. Biomaterials. 2003 Feb;24(3):401-16. doi: 10.1016/s0142-9612(02)00353-8. PMID: 12423595.
41. Masini BD, Stinner DJ, Waterman SM, Wenke JC. Bacterial adherence to high--tensile strength sutures. Arthroscopy. 2011 Jun;27(6):834-8. doi: 10.1016/j.arthro.2011.02.003. PMID: 21624678.
42. Tomita N, Tamai S, Morihara T, Ikeuchi K, Ikada Y. Handling characteristics of braided suture materials for tight tying. J Appl Biomater. 1993 Spring;4(1):61-5. doi: 10.1002/jab.770040108. PMID: 10148347.
43. Viju S, Thilagavathi G. Characterization of tetracycline hydrochloride drug incorporated silk sutures. J Text Inst 2013; 104:289–94.
44. Postlethwait RW, Willigan DA, Ulin AW. Human tissue reaction to sutures. Ann Surg. 1975 Feb;181(2):144-50. doi: 10.1097/00000658-197502000-00003. PMID: 122890; PMCID: PMC1343743.
45. Byrne M, Aly A. The Surgical Suture. Aesthet Surg J. 2019 Mar 14;39(Suppl_2):S67-S72. doi: 10.1093/asj/sjz036. PMID: 30869751.
46. Numata K, Kaplan DL. Silk-based gene carriers with cell membrane destabilizing peptides. Biomacromolecules 2010; 11:3189–95.
47. Numata K, Hamasaki J, Subramanian B, Kaplan DL. Gene delivery mediated by recombinant silk proteins containing cationic and cell binding motifs. J Controlled Release 2010; 146:136–43
48. Pritchard EM, Kaplan DL. Silk fibroin biomaterials for controlled release drug delivery. Expert Opin Drug Deliv 2011; 8:797–811
49. 178] Parker ST, Domachuk P, Amsden J, Bressner J, Lewis JA, Kaplan DL, Omenetto FG. Biocompatible silk printed optical waveguides. Adv Mater 2009; 21:2411–5
50. Capelli R, Amsden JJ, Generali G, Toffanin S, Benfenati V, Muccini M, Kaplan DL, Omenetto FG, Zamboni R. Integration of silk protein in organic and light-emitting transistors. Org Electron 2011; 12:1146–51.
51. Tansil NC, Koh LD, Han MY. Functional silk: colored and luminescent. Adv Mater 2012; 24:1388–97.
52. Müller C, Hamedi M, Karlsson R, Jansson R, Marcilla R, Hedhammar M, Inganäs O. Woven electrochemical transistors on silk fibers. Adv Mater 2011; 23:898–901.
53. Aznar-Cervantes S, Roca MI, Martinez JG, Meseguer-Olmo L, Cenis JL, Moraleda JM, Otero TF. Fabrication of conductive electrospun silk fibroin scaffolds by coating with polypyrrole for biomedical applications. Bioelectrochemistry 2012; 85:36–43.

54. Sahoo JK, Hasturk O, Falcucci T, Kaplan DL. Silk chemistry and biomedical material designs. Nat Rev Chem. 2023 May;7(5):302-318. doi: 10.1038/s41570-023-00486-x. Epub 2023 Apr 21. PMID: 37165164.
55. Li, C. et al. Design of biodegradable, implantable devices towards clinical translation. Nat. Rev. Mater. 5, 61–81 (2020).
56. Buckwalter, J.A.; Glimcher, M.J.; Cooper, R.R.; Recker, R. Bone biology. I: Structure, blood supply, cells, matrix, and mineralization. Instr. Course Lect. 1996, 45, 371–386.
57. Roach, H.I. Why does bone matrix contain non-collagenous proteins? The possible roles of osteocalcin, osteonectin, osteopontin and bone sialoprotein in bone mineralisation and resorption. Cell Biol. Int. 1994, 18, 617–628.
58. Frantz, C.; Stewart, K.M.;Weaver, V.M. The extracellular matrix at a glance. J. Cell Sci. 2010, 123, 4195–4200
59. Kasoju, N.; Bora, U. Silk fibroin in tissue engineering. Adv. Healthc. Mater. 2012, 1, 393–412
60. Meinel, L.; Hofmann, S.; Betz, O.; Fajardo, R.; Merkle, H.P.; Langer, R.; Evans, C.H.; Vunjak-Novakovic, G.; Kaplan, D.L. Osteogenesis by human mesenchymal stem cells cultured on silk biomaterials: Comparison of adenovirus mediated gene transfer and protein delivery of BMP-2. Biomaterials 2006, 27, 4993–5002
61. Ding, X.; Wei, X.; Huang, Y.; Guan, C.; Zou, T.; Wang, S.; Liu, H.; Fan, Y. Delivery of demineralized bone matrix powder using a salt-leached silk fibroin carrier for bone regeneration. J. Mater. Chem. B 2015, 3, 3177–3188
62. Chung, C.; Burdick, J.A. Engineering cartilage tissue. Adv. Drug Deliv. Rev. 2008, 60, 243–262.
63. Huey, D.J.; Hu, J.C.; Athanasiou, K.A. Unlike Bone, Cartilage Regeneration Remains Elusive. Science 2012, 338, 917–921.
64. Bhardwaj, N.; Singh, Y.P.; Devi, D.; Kandimalla, R.; Kotoky, J.; Mandal, B.B. Potential of silk fibroin/chondrocyte constructs of muga silkworm Antheraea assamensis for cartilage tissue engineering. J. Mater. Chem. B 2016, 4, 3670–3684
65. Uebersax, L.; Merkle, H.P.; Meinel, L. Insulin-like growth factor I releasing silk fibroin scaffolds induce chondrogenic differentiation of human mesenchymal stem cells. J. Control. Release 2008, 127, 12–21.
66. Ding, F.; Deng, H.; Du, Y.; Shi, X.; Wang, Q. Emerging chitin and chitosan nanofibrous materials for biomedical applications. Nanoscale 2014, 6, 9477–9493.
67. Lien, S.-M.; Ko, L.-Y.; Huang, T.-J. Effect of pore size on ECM secretion and cell growth in gelatin scaffold for articular cartilage tissue engineering. Acta Biomater. 2009, 5, 670–679
68. Zhang, X.; Reagan, M.R.; Kaplan, D.L. Electrospun silk biomaterial scaffolds for regenerative medicine. Adv. Drug Deliv. Rev. 2009, 61, 988–1006
69. Uttayarat, P.; Jetawattana, S.; Suwanmala, P.; Eamsiri, J.; Tangthong, T.; Pongpat, S. Antimicrobial electrospun silk fibroin mats with silver nanoparticles for wound dressing application. Fibers Polym. 2012, 13, 999–1006.
70. Farokhi, M.; Mottaghitalab, F.; Fatahi, Y.; Khademhosseini, A.; Kaplan, D.L. Overview of Silk Fibroin Use inWound Dressings. Trends Biotechnol. 2018, 36, 907–922.
71. Kong, M.; Chen, X.G.; Xing, K.; Park, H.J. Antimicrobial properties of chitosan and mode of action: A state of the art review. Int. J. Food Microbiol. 2010, 144, 51–63.
72. Cai, Z.-X.; Mo, X.-M.; Zhang, K.-H.; Fan, L.-P.; Yin, A.-L.; He, C.-L.;Wang, H.-S. Fabrication of Chitosan/Silk Fibroin Composite Nanofibers forWound-dressing Applications. Int. J. Mol. Sci. 2010, 11, 3529–3539.
73. Xu, Y.; Li, L.; Yu, X.; Gu, Z.; Zhang, X. Feasibility study of a novel crosslinking reagent (alginate dialdehyde) for biological tissue fixation. Carbohydr. Polym. 2012, 87, 1589–1595

74. Allardyce, B.J.; Rajkhowa, R.; Dilley, R.J.; Xie, Z.; Campbell, L.; Keating, A.; Atlas, M.D.; von Unge, M.;Wang, X. Comparative acoustic performance and mechanical properties of silk membranes for the repair of chronic tympanic membrane perforations.J. Mech. Behav. Biomed. Mater. 2016, 64, 65–74.
75. Kuo, C.K.; Marturano, J.E.; Tuan, R.S. Novel strategies in tendon and ligament tissue engineering: Advanced biomaterials and regeneration motifs. BMC Sports Sci. Med. Rehabil. 2010, 2, 20.
76. Tatara, A.M.; Mikos, A.G. Tissue Engineering in Orthopaedics. J. Bone Jt. Surg. Am. 2016, 98, 1132–1139.
77. Kundu, B.; Rajkhowa, R.; Kundu, S.C.; Wang, X. Silk fibroin biomaterials for tissue regenerations. Adv. Drug Deliv. Rev. 2013, 65, 457–470.
78. Altman, G.H.; Horan, R.L.; Lu, H.H.; Moreau, J.; Martin, I.; Richmond, J.C.; Kaplan, D.L. Silk matrix for tissue engineered anterior cruciate ligaments. Biomaterials 2002, 23, 4131–4141.
79. Liu, H.; Fan, H.;Wang, Y.; Toh, S.L.; Goh, J.C.H. The interaction between a combined knitted silk scaffold and microporous silk sponge with human mesenchymal stem cells for ligament tissue engineering. Biomaterials 2008, 29, 662–674.
80. Li G, Sun S. Silk Fibroin-Based Biomaterials for Tissue Engineering Applications. Molecules. 2022 Apr 25;27(9):2757. doi: 10.3390/molecules27092757. PMID: 35566110; PMCID: PMC9103528.
81. Nguyen TP, Nguyen QV, Nguyen VH, Le TH, Huynh VQN, Vo DN, Trinh QT, Kim SY, Le QV. Silk Fibroin-Based Biomaterials for Biomedical Applications: A Review. Polymers (Basel). 2019 Nov 24;11(12):1933. doi: 10.3390/polym11121933. PMID: 31771251; PMCID: PMC6960760.
82. G.H. Altman, R.L. Horan, H.H. Lu, J. Moreau, I. Martin, J.C. Richmond, D.L. Kaplan, Silk matrix for tissue engineered anterior cruciate ligaments, Biomaterials 23 (2002) 4131- 4141.
83. R. Ahmad, A. Kamra, S.E. Hasnain, Fibroin silk proteins from the nonmulberry silkworm Philosamia ricini are biochemically and immunologically distinct from those of the mulberry silkworm Bombyx mori, DNA Cell Biol. 23 (2004) 149–154
84. C. Acharya, B. Hinz, S.C. Kundu, The effect of lactose-conjugated silk biomaterials on the development of fibrogenic fibroblast, Biomaterials 29 (2008) 4665–4675.
85. N.V. Bhat, S.M. Ahirrao, Investigation of the structure of silk film regenerated with lithium thiocyanate solution, J. Polym. Sci. Part A: Polym. Chem. 21 (1983) 1273–1280
86. W. Tao, M. Li, C. Zhao, Structure and properties of regenerated Antheraea pernyi silk fibroin in aqueous solution, Int. J. Biol. Macromol. 40 (2007) 472–478.
87. H. Kweon, Y.H. Park, Dissolution and characterization of regenerated Antheraea pernyi silk fibroin, J. Appl. Polym. Sci. 82 (2001) 750–758.
88. I.C. Um, H. Kweon, Y.H. Park, S. Hudson, Structural characteristics and properties of the regenerated silk fibroin prepared from formic acid, Int. J. Biol. Macromol. 29 (2001) 91–97.
89. M.K. Gupta, S.K. Khokhar, D.M. Phillips, L.A. Sowards, L.F. Drummy, M.P. Kadakia, R.R. Naik, Patterned silk films cast from ionic liquid solubilized fibroin as scaffolds for cell growth, Langmuir 23 (2006) 1315–1319.
90. A. Higuchi, M. Yoshida, T. Ohno, T. Asakura, M. Hara, Production of interferon-β in a culture of fibroblast cells on some polymeric films, Cytotechnology 34 (2000) 165–173.
91. X. Wang, H.J. Kim, P. Xu, A. Matsumoto, D.L. Kaplan, Biomaterial coatings by stepwise deposition of silk fibroin, Langmuir 21 (2005) 11335–11341
92. Q. Lu, X. Hu, X. Wang, J.A. Kluge, S. Lu, P. Cebe, D.L. Kaplan, Water-insoluble silk films with silk I structure, Acta Biomater. 6 (2010) 1380–1387.
93. X. Zhang, M.R. Reagan, D.L. Kaplan, Electrospun silk biomaterial scaffolds for regenerative medicine, Adv. Drug Deliv. Rev. 61 (2009) 988–1006
94. B.D. Lawrence, Z. Pan, M.D. Weber, D.L. Kaplan, M.I. Rosenblatt, Silk film culture system for in vitro analysis and biomaterial Design, J. Vis. Exp. (2012) 3646.

95. Ahmed, E.M. Hydrogel: Preparation, characterization, and applications: A review. J. Adv. Res. 2015, 6, 105–121. [CrossRef] [PubMed]
96. X. Chen, W. Li, W. Zhong, Y. Lu, T. Yu, pH sensitivity and ion sensitivity of hydrogels based on complex-forming chitosan/silk fibroin interpenetrating polymer network, J. Appl. Polym. Sci. 65 (1997) 2257–2262.
97. A. Motta, C. Migliaresi, F. Faccioni, P. Torricelli, M. Fini, R. Giardino, Fibroin hydrogels for biomedical applications: preparation, characterization and in vitro cell culture studies, J. Biomater. Sci. Polym. Ed. 15 (2004) 851–864.
98. N. Guziewicz, A. Best, B. Perez-Ramirez, D.L. Kaplan, Lyophilized silk fibroin hydrogels for the sustained local delivery of therapeutic monoclonal antibodies, Biomaterials 32 (2011) 2642-2650.
99. U.J. Kim, J. Park, C. Li, H.-J. Jin, R. Valluzzi, D.L. Kaplan, Structure and properties of silk hydrogels, Biomacromolecules 5 (2004) 786–792.
100. P.H. Chao, S. Yodmuang, X. Wang, L. Sun, D.L. Kaplan, Silk hydrogel for cartilage tissue engineering, J. Biomed. Mater. Res. B Appl. Biomater. (2010) 84–90.
101. J.H. Yeo, K.G. Lee, Y.W. Lee, S.Y. Kim, Simple preparation and characteristics of silk fibroin microsphere, Eur. Polym. J. 39 (2003) 1195–1199.
102. E. Wenk, A.J. Wandrey, H.P. Merkle, L. Meinel, Silk fibroin spheres as a platforfor controlled drug delivery, J. Control. Release 132 (2008) 26–34.
103. A.S. Lammel, X. Hu, S.H. Park, D.L. Kaplan, T.R. Scheibel, Controlling silk fibroin particle features for drug delivery, Biomaterials 31 (2010) 4583–4591.
104. Y.Q. Zhang, S. Wei-De, X. Ru-Li, L.J. Zhuge, W.J. Gao, W.B. Wang, Formation of silk nanoparticles in water-miscible organic solvent and their characterization,nJ. Nanopart. Res. 9 (2007) 885–900.
105. Z. Cao, X. Chen, J. Yao, L. Huang, Z. Shao, The preparation of regenerated silk fibroin microspheres, Soft Matter 3 (2007) 910–915
106. R. Rajkhowa, E.S. Gil, J.A. Kludge, K. Numata, L. Wang, X. Wang, D.L. Kaplan, Reinforcing silk scaffolds with silk particles, Macromol. Biosci. 10 (2010) 599–611.
107. Zhou, Z.T.; Zhang, S.Q.; Cao, Y.T.; Marelli, B.; Xia, X.X.; Tao, T.H. Engineering the Future of Silk Materials through Advanced Manufacturing. Adv. Mater. 2018, 30, 1706983.
108. Whitesides, G.M.; Ostuni, E.; Takayama, S.; Jiang, X.; Ingber, D.E. Soft lithography in biology and biochemistry. Annu. Rev. Biomed. Eng. 2001, 3, 335–373.
109. Jose, R.R.; Rodriguez, M.J.; Dixon, T.A.; Omenetto, F.; Kaplan, D.L. Evolution of Bioinks and Additive Manufacturing Technologies for 3D Bioprinting. ACS Biomater. Sci. Eng. 2016, 2, 1662–1678.
110. Murphy, S.V.; Atala, A. 3D bioprinting of tissues and organs. Nat. Biotechnol. 2014, 32, 773–785.
111. Kim, U.J.; Park, J.; Kim, H.J.; Wada, M.; Kaplan, D.L. Three-dimensional aqueous derived biomaterial scaffolds from silk fibroin. Biomaterials 2005, 26, 2775–2785.
112. Tamada, Y. New process to form a silk fibroin porous 3-D structure. Biomacromolecules 2005, 6, 3100–3106.
113. Nazarov, R.; Jin, H.J.; Kaplan, D.L. Porous 3-D scaffolds from regenerated silk fibroin. Biomacromolecules 2004, 5, 718–726.
114. Tsukada, M.; Freddi, G.; Minoura, N.; Allara, G. Preparation and Application of Porous Silk Fibroin Materials. J. Appl. Polym. Sci. 1994, 54, 507–514.
115. Kapałczyńska M, Kolenda T, Przybyła W, Zajączkowska M, Teresiak A, Filas V, Ibbs M, Bliźniak R, Łuczewski Ł, Lamperska K. 2D and 3D cell cultures - a comparison of different types of cancer cell cultures. Arch Med Sci. 2018 Jun;14(4):910-919. doi: 10.5114/aoms.2016.63743. Epub 2016 Nov 18. PMID: 30002710; PMCID: PMC6040128.
116. Pampaloni F, Reynaud EG, Stelzer EH. The third dimension bridges the gap between cell culture and live tissue. Nat Rev Mol Cell Biol. 2007;8:839–45. [PubMed] [Google Scholar]

117. Baker B, Chen C. Deconstructing the third dimension – how 3D culture microenvironments alter cellular cues. J Cell Sci. 2012;125:3015–24. [PMC free article] [PubMed] [Google Scholar]
118. Hickman JA, Graeser R, de Hoogt R, et al. Three-dimensional models of cancer for pharmacology and cancer cell biology: capturing tumor complexity in vitro/ex vivo. Biotechnol J. 2014;9:1115–28. [PubMed] [Google Scholar]
119. Bissell MJ, Rizki A, Mian IS. Tissue architecture: the ultimate regulator of breast epithelial function. Curr Opin Cell Biol. 2003;15:753–62. [PMC free article] [PubMed] [Google Scholar]
120. von der Mark K, Gauss V, von der Mark H, Müller P. Relationship between cell shape and type of collagen synthesised as chondrocytes lose their cartilage phenotype in culture. Nature. 1977;267:531–2. [PubMed] [Google Scholar]
121. Petersen OW, Rønnov-Jessen L, Howlett AR, Bissel MJ. Interaction with basement membrane serves to rapidly distinguish growth and differentiation pattern of normal and malignant human breast epithelial cells. Proc Natl Acad Sci USA. 1992;89:9064–8. [PMC free article] [PubMed] [Google Scholar]
122. Mahmud G, Campbell CJ, Bishop KJM, et al. Directing cell motions on micropatterned ratchets. Nat Phys. 2009;5:606–12. [Google Scholar]
123. Kilian K, Bugarija B, Lahn BT, et al. Geometric cues for directing the differentiation of mesenchymal stem cells. Proc Natl Acad Sci USA. 2010;107:4872–7. [PMC free article] [PubMed] [Google Scholar]
124. Debnath J, Brugge JS. Modelling glandular epithelial cancers in three-dimensional cultures. Nat Rev Cancer. 2005;5:675–88. [PubMed] [Google Scholar]
125. Nelson CM, Bissell MJ. Of extracellular matrix, scaffolds, and signaling: tissue architecture regulates development, homeostasis, and cancer. Annu Rev Cell Dev Biol. 2006;22:287–309. [PMC free article] [PubMed] [Google Scholar]
126. Mseka T, Bamburg JR, Cramer LP. ADF/cofilin family proteins control formation of oriented actin-filament bundles in the cell body to trigger fibroblast polarization. J Cell Sci. 2007;120:4332–44. [PubMed] [Google Scholar]
127. Weaver V, Lelièvre S, Lakins JN, et al. Beta4 integrin-dependent formation of polarized three-dimensional architecture confers resistance to apoptosis in normal and malignant mammary epithelium. Cancer Cell. 2002;2:205–16. [PMC free article] [PubMed] [Google Scholar]
128. Meyers J, Craig J, Odde DJ. Potential for control of signaling pathways via cell size and shape. Curr Biol. 2003;16:1685–93. [PubMed] [Google Scholar]
129. Kumari N, Pullaguri N, Sahu V, Ealla KKR. Research and therapeutic applications of silk proteins in cancer. Journal of Biomaterials Applications. 2023;38(1):39-50. doi:10.1177/08853282231184572
130. Kumari N, Bhargava A, Rath SN. T-type calcium channel antagonist, TTA-A2 exhibits anti-cancer properties in 3D spheroids of A549, a lung adenocarcinoma cell line. Life Sci 2020; 260: 118291.
131. Abbott A, Bond K, Chiba T, et al. Development of a mechanically matched silk scaffolded 3D clear cell renal cell carcinoma model. Mater Sci Eng C 2021; 126: 112141.
132. Dondajewska E, Juzwa W, Mackiewicz A, et al. Heterotypic breast cancer model based on a silk fibroin scaffold to study the tumor microenvironment. Oncotarget 2018; 9: 4935–4950.
133. Mishra A, Mukhopadhyay SK, Dey S. Evaluation of cyclosaplin efficacy using a silk based 3D tumor model. Biomolecules 2019; 9: 123.
134. Duval K, Grover H, Han L-H, et al. Modeling physiological events in 2D vs. 3D cell culture. Physiology 2017; 32: 266–277.
135. Gurski LA, Petrelli NJ, Jia X, et al. 3D matrices for anti-cancer drug testing and development. Oncol Issues 2010; 25: 20–25.
136. Langhans SA (2018) Three-Dimensional in Vitro Cell Culture Models in Drug Discovery and Drug Repositioning. Front. Pharmacol. 9:6. doi: 10.3389/fphar.2018.00006

137. Mueller-Klieser, W. (1987). Multicellular spheroids. A review on cellular aggregates in cancer research. J. Cancer Res. Clin. Oncol. 113, 101–122. doi: 10.1007/BF00391431
138. Cukierman, E., Pankov, R., Stevens, D. R., and Yamada, K. M. (2001). Taking cell-matrix adhesions to the third dimension. Science 294, 1708–1712. doi: 10.1126/science.1064829
139. Campos, L. S. (2004). Neurospheres: insights into neural stem cell biology. J. Neurosci. Res. 78, 761–769. doi: 10.1002/jnr.20333
140. Stadler, M.,Walter, S.,Walzl, A., Kramer, N., Unger, C., Scherzer, M., et al. (2015). Increased complexity in carcinomas: analyzing and modeling the interaction of human cancer cells with their microenvironment. Semin. Cancer Biol. 35:107–124. doi: 10.1016/j.semcancer.2015.08.007
141. Friedrich, J., Seidel, C., Ebner, R., and Kunz-Schughart, L. A. (2009). Spheroidbased drug screen: considerations and practical approach. Nat. Protoc. 4, 309–324. doi: 10.1038/nprot.2008.226
142. Ivascu, A., and Kubbies, M. (2006). Rapid generation of single-tumor spheroids for high-throughput cell function and toxicity analysis. J. Biomol. Screen. 11, 922–932. doi: 10.1177/1087057106292763
143. Souza, G. R., Molina, J. R., Raphael, R. M., Ozawa, M. G., Stark, D. J., Levin, C. S., et al. (2010). Three-dimensional tissue culture based on magnetic cell levitation. Nat. Nanotechnol. 5, 291–296. doi: 10.1038/nnano.2010.23
144. Timm, D. M., Chen, J., Sing, D., Gage, J. A., Haisler, W. L., Neeley, S. K., et al. (2013). A high-throughput three-dimensional cell migration assay for toxicity screening with mobile device-based macroscopic image analysis. Sci. Rep. 3:3000. doi: 10.1038/srep03000
145. Abuwatfa, W.H., Pitt, W.G. & Husseini, G.A. Scaffold-based 3D cell culture models in cancer research. J Biomed Sci 31, 7 (2024). https://doi.org/10.1186/s12929-024-00994-y<
146. Santos SC, Custódio CA, Mano JF. Human protein-based porous scaffolds as platforms for xeno-free 3D cell culture. Adv Healthc Mater. 2022;11(12).
147. Afewerki S, Sheikhi A, Kannan S, Ahadian S, Khademhosseini A. Gelatin-polysaccharide composite scaffolds for 3D cell culture and tissue engineering: Towards natural therapeutics. Bioeng Transl Med. 2018;4(1):96–115.
148. Ravi M, Paramesh V, Kaviya SR, Anuradha E, Paul Solomon FD. 3D cell culture systems: advantages and applications. J Cell Physiol. 2015;230(1):16–26. https:// doi. org/ 10. 1002/ jcp. 24683.
149. Pradhan S, Clary JM, Seliktar D, Lipke EA. A three-dimensional spheroidal cancer model based on PEG-fibrinogen hydrogel microspheres. Biomaterials. 2017;1(115):141–54.
150. Alépée, N., Bahinski, A., Daneshian, M., De Wever, B., Fritsche, E., Goldberg, A., et al. (2014). State-of-the-art of 3D cultures (organs-on-a-chip) in safety testing and pathophysiology. ALTEX 31, 441–477. doi: 10.14573/altex1406111
151. Simian, M., and Bissell, M. J. (2017). Organoids: a historical perspective of thinking in three dimensions. J. Cell Biol. 216, 31–40. doi: 10.1083/jcb.2016 10056
152. Clevers, H. (2016). Modeling development and disease with organoids. Cell 165, 1586–1597. doi: 10.1016/j.cell.2016.05.082
153. Fatehullah, A., Tan, S. H., and Barker, N. (2016). Organoids as an in vitro model of human development and disease. Nat. Cell Biol. 18, 246–254. doi: 10.1038/ncb3312
154. Xu, X., Farach-Carson, M. C., and Jia, X. (2014). Three-dimensional in vitro tumor models for cancer research and drug evaluation. Biotechnol. Adv. 32, 1256–1268. doi: 10.1016/j.biotechadv.2014.07.009
155. Ferlay J, Soerjomataram I, Dikshit R, Eser S, Mathers C, Rebelo M, Parkin DM, Forman D, Bray F. Cancer incidence and mortality worldwide: sources, methods and major patterns in GLOBOCAN 2012. Int J Cancer. 2015 Mar 1;136(5): E359-86. doi: 10.1002/ijc.29210. Epub 2014 Oct 9. PMID: 25220842.
156. Miyazawa, T.; Blout, E. R. J. Am. Chem. Soc.1961, 83, 712−719.

157. Cho HJ, Ki CS, Oh H, Lee KH, Um IC. Molecular weight distribution and solution properties of silk fibroins with different dissolution conditions. Int J Biol Macromol. 2012 Oct;51(3):336–41.
158. Rnjak-Kovacina J, Wray LS, Burke KA, Torregrosa T, Golinski JM, Huang W, et al. Lyophilized Silk Sponges: A Versatile Biomaterial Platform for Soft Tissue Engineering. ACS Biomater Sci Eng. 2015 Apr 13;1(4):260–70.
159. Wang HY, Zhang YQ. Effect of regeneration of liquid silk fibroin on its structure and characterization. Soft Matter. 2013;9(1):138–45.